CZECH TECHNICAL
UNIVERSITY
IN PRAGUE

F3

Faculty of Electrical Engineering
Department of Microelectronics

Bachelor's Thesis

Applications of Atomic Layer Deposition for the structures of photovoltaic cells

Ruslanbek Ablataev
Open Electronic Systems

May 2022
Supervisor: doc.RNDr. Jan Voves, Csc

BACHELOR‘S THESIS ASSIGNMENT

I. Personal and study details

Student's name: **Ablataev Ruslanbek** Personal ID number: **478024**

Faculty / Institute: **Faculty of Electrical Engineering**

Department / Institute: **Department of Radioelectronics**

Study program: **Open Electronic Systems**

II. Bachelor’s thesis details

Bachelor’s thesis title in English:

Applications of Atomic Layer Deposition for the structures of photovoltaic cells.

Bachelor’s thesis title in Czech:

Aplikace depozice atomárních vrstev pro struktury fotovoltaických článků

Guidelines:

1. Study the principles of Atomic Layer Deposition (ALD) and possible applications in the photovoltaic cell technology.
2. Choose the suitable dielectric layer for the improvement of the photovoltaic cell parameters.
3. Grow the chosen layer and characterize its properties.

Bibliography / sources:

[1] J. A. van Delft, D. Garcia-Alonso, W. M. M. Kessels: Atomic layer deposition for photovoltaics: Applications and prospects for solar cell manufacturing, Semiconductor Science and Technology, vol. 27, p. 074002, 2012
[2] M. A. Hossain, K. T. Khoo, G. K. Poduval, T. Zhang, X. Li, W. M. Li, B. Hoex: Atomic layer deposition enabling higher efficiency solar cells: A review, Nano Materials Science, vol. 2, p. 204-226, 2020
[3] R. W. Johnson, A. Hultqvist, S. F. Bent: A brief review of atomic layer deposition: from fundamentals to applications, Materials Today, vol. 17, No. 5, 2014

Name and workplace of bachelor’s thesis supervisor:

doc. RNDr. Jan Voves, CSc. Department of Microelectronics FEE

Name and workplace of second bachelor’s thesis supervisor or consultant:

Date of bachelor’s thesis assignment: **27.01.2022** Deadline for bachelor thesis submission: **20.05.2022**

Assignment valid until: **30.09.2023**

doc. RNDr. Jan Voves, CSc.	doc. Ing. Stanislav Vítek, Ph.D.	prof. Mgr. Petr Páta, Ph.D.
Supervisor’s signature	Head of department’s signature	Dean’s signature

III. Assignment receipt

The student acknowledges that the bachelor’s thesis is an individual work. The student must produce his thesis without the assistance of others, with the exception of provided consultations. Within the bachelor’s thesis, the author must state the names of consultants and include a list of references.

.	
Date of assignment receipt	Student’s signature

Acknowledgement / Declaration

I would like to thank Jan Voves for giving me an opportunity to participate in the nanofabrication process, for his support in writing this thesis and patience. I would like to thank all members of the ALD research team for their guidance and advice. I want to thank my family and friends for the support and for giving me an opportunity to focus on my studies.

I declare that I completed the presented thesis independently and that all used sources are quoted in accordance with the Methodological instructions that cover the ethical principles for writing an academic thesis.

In Prague, 18. May 2022

.....

Abstrakt / Abstract

Atomic layer deposition (ALD) je metoda depozice z plynné fáze, která umožňuje nanášení tenkých nanometrových vrstev materialu bez drobných otvorů. Díky samoomezujícím reakcím zahrnutým v procesu, ALD poskytuje vynikající konformitu, nízké teploty nanášení a přesnou kontrolu tloušťky a složení. Díky miniaturizaci v elektronickém průmyslu, zejména ve výrobě fotovoltaických zařízení, ALD získalo významný zájem. Úprava rozhraní, která je klíčová pro získání efektivních fotovoltaických článků, může být přesně provedena pomocí metody ALD a byla zkoumána pro různé typy fotovoltaických zařízení. Tato bakalárská práce představuje hlavní principy ALD a ukazuje jej výhody. Dále je uveden přehled aplikací ALD při výrobě fotovoltaických článků. Experimentální část této práce je zaměřena na depozici vrstev oxidu hlinitého Al_2O_3 na Si wafer a následnou analýzu zlepšených fotovoltaických vlastností.

Klíčová slova: Depozice atomárních vrstev; Fotovoltaický článek; Aplikace; Pasivace; Křemíkový wafer; Oxid hlinitý;

Překlad titulu: Aplikace depozice atomárních vrstev pro struktury fotovoltaických článků

Atomic layer deposition (ALD) is a gas/vapor phase technique that allows depositing pinhole-free nanoscale thin films. Due to the self-limiting reactions involved in the process, ALD provides excellent conformality, low deposition temperatures, and precise thickness and composition control. Due to miniaturization in the electronics industry, particularly photovoltaic device manufacturing, ALD has gained significant traction. Interface modification, which is crucial for obtaining effective solar cells, can be accurately done using the ALD method, and it has been explored for various types of photovoltaic devices. This thesis introduces the main principles of ALD and showcases its benefits. Then an overview of ALD applications in photovoltaic device fabrication is given. The experimental part of this thesis focuses on the deposition of aluminum oxide Al_2O_3 layers onto Si wafer and subsequent analysis of improved photovoltaic characteristics.

Keywords: Atomic layer deposition; Photovoltaic cell; Applications; Passivation; Silicon wafer; Aluminum oxide;

Contents /

Tables / Figures

Chapter 1
Introduction

Atomic Layer Deposition (ALD) is a sequential self-limiting gas/vapor deposition process that allows the fabrication of conformal pinhole-free nanoscale films. ALD is a unique method that has attracted much traction due to its advantageous properties, such as high conformality and uniformity of deposited films, precise control over thickness and composition, and low deposition temperatures. ALD has shown promise in the semiconductor industry and energy harvesting technologies, such as solar cells.

The performance of photovoltaic devices is strongly dependent on interface properties between various layers. Thus interface engineering methods are crucial to achieving high power conversions [15]. ALD is a powerful deposition method that can precisely control the growth and composition of the deposited films, tuning properties of the interfaces to desired qualities. The implementation of ALD into solar cells has been proceeding since the 1990s and includes the manufacturing of passivation layers, buffer layers, absorber layers, selective contacts, protective coatings, etc [7]. Currently, ALD has been used mainly in academic research and gradually introduced into the commercial fabrication of photovoltaic devices.

This thesis aims to introduce the basic principles of ALD, outline parameters important to successful deposition, and highlight ALD's natural advantages over other deposition methods. A showcase of ALD applications in photovoltaic device manufacturing is then given. The later chapter focuses on making a case for the aluminum oxide layer as the suitable passivation layer for Si-based solar cells. The experimental part of the thesis focuses on the fabrication of Al_2O_3 layers and their subsequent characterization with the Atomic Force Microscopy (AFM) and effective lifetime measurements.

1.1 Origination of ALD

It can be stated that ALD has been introduced twice independently of each other. Initially, prof.Valentin Borisovich Aleskovsky of Leningrad Institute of Technology and prof.Stanislav Ivanovich Koltsov experimentally developed the principles of ALD and, in 1965, published the principles of ALD under the title of "Molecular Layering" [16]. Later in1974, professor Tuomo Suntola devised the first iteration of ALD as the Atomic Layer Epitaxy (ALE) at Instrumentarium Oy, Finland [17]. Later in the 1980s, research on ALE application focused on the deposition of II-VI and III-V semiconductors using organometallic compounds, simultaneously further extending the library of available chemical elements for deposition. As prof.Suntola continued to improve the deposition method, introducing more metals and fabricating more metal oxides, which were deposited non-epitaxially, the method has distinguished itself as Atomic Layer Deposition (ALD). In the late 1990s and early 2000s, the method found exciting applications for the production of silicon-based electronics as a result of the ever-increasing miniaturization of electronic device dimensions [18].

1.2 Comparison of ALD with CVD and other deposition methods

Main film deposition methods can be divided into three groups: gas, liquid, and solid-based deposition methods. The deposition method also can be either physical or chemical. These methods include Physical Vapor Deposition (PVD) and its modification: Molecular Beam Epitaxy (MBE), Pulsed Laser Deposition (PLD); as well as Chemical Vapor Deposition (CVD) and its modifications Low-Pressure CVD (LPCVD), Metal-Organic CVD (MOCVD) [16]. PVD is a top-down method that uses condensation of gaseous source material on the substrate to form thin films. CVD is a bottom-up method involving chemical reactions conducted by volatile precursor molecules [2]. These molecules are simultaneously introduced into the chamber, where they decompose at the surface, which is usually heated to stimulate reactions and leave a thin film of the desired material.

For many ALD methods, different CVD and MOCVD served as a template [1, 19]. However, the ALD process features alternating exposure of chemical precursors at lower temperatures with a self-saturating reaction, leading to controlled growth, hence differing from CVD [2]. Unique qualities of ALD, such as excellent uniformity and conformality, precise thickness control, and low-temperature depositions, distinguish ALD from other deposition methods and give it leverage. These advantages are given by several reasons: unlike CVD and PVD, ALD has a lesser dependence on the flux control of the precursor. Flux-controlled process growth rate, uniformity, and conformality are directly related to the flux of source species and thus require precise flux regulation to optimize the deposition [2]. The self-limiting nature of surface reactions is another reason. As a comparison, Pulsed Chemical Vapor Deposition (PCVD) likewise uses alternating exposure of chemical precursors, separated by purge periods, but unlike ALD, the growth rate does not reach saturation with the increasing flow rate of co-reactants during respective pulses [19]. Another improvement over other methods is that during ALD reactor chamber is purged after every introduction of precursor, which improves uniformity and restricts the incorporation of reaction by-products as impurities in the deposited film, lowering defect density [19].

Chapter 2
Principles of ALD

2.1 Description of ALD

Due to self-limited reactions between precursors and substrate, ALD has been classified as a self-assembly process in the International Technology Roadmap for Semiconductors (ITRS) [5]. ALD is a gas/vapor deposition method, where in a sequence of alternating self-limiting surface reactions a film of desired materials is created. Precursors are introduced into reactor chamber sequentially and separately. Precursor species react only with accessible surface active sites, which are consumed as reaction proceeds [19]. Once the surface has been depleted of all the accessible active sites, the reaction stops regardless of the existence of excess precursor molecules, creating a sub-monolayer of the deposited material. The reactor is then purged, and a subsequent reactant is introduced. A number of sequences compose a single cycle, during which a single monolayer of the film is deposited. Cycles are repeated a discrete number of times until desired thickness has been achieved [2]. Sequential behavior of ALD provides an opportunity for precise control and tunability.

2.1.1 Description of ALD process

ALD process consists of a discrete number of cycles, which are conducted under certain deposition conditions specified by an ALD material recipe [19].

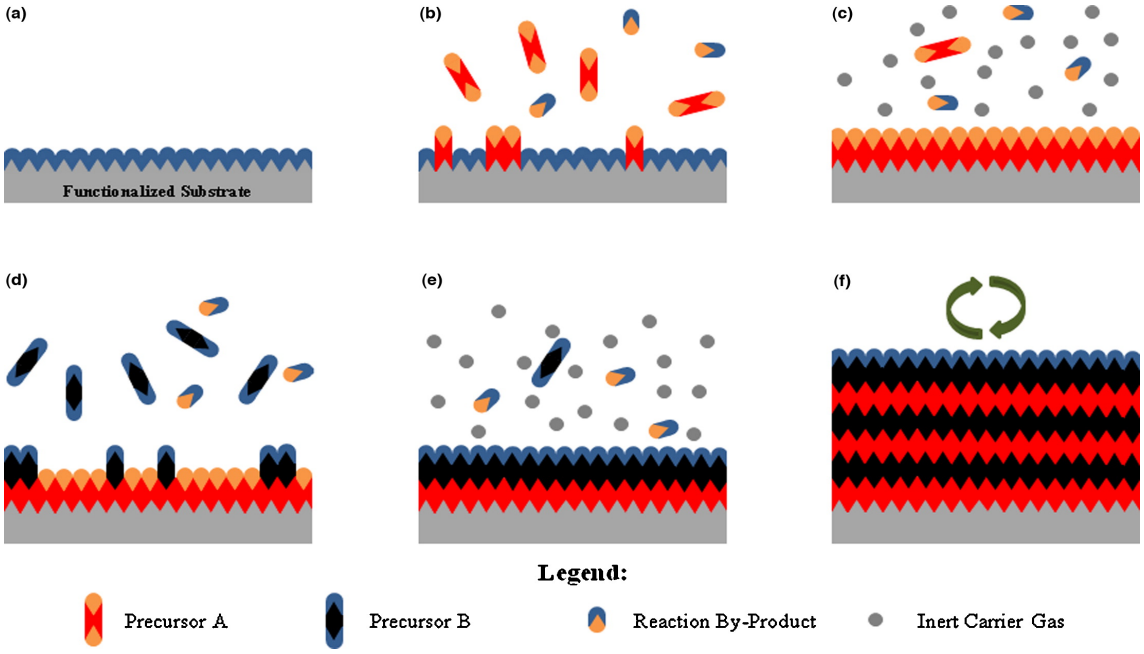

Figure 2.1. Schematics of ALD process (a) functionalized substrate prior to deposition, (b) exposure to precursor A and its reaction with the surface, (c) first purge sequence, (d) exposure to precursor B and its reaction with the newly created sub-monolayer, (e) second purge sequence, (f) repeated cycles of ALD process [1].

Each cycle, in general, consists of 4 steps. It is essential, as it is depicted in Fig. 2.1 (a), to confirm that the substrate surface is functionalized or treated to functionalize in chemical reactions with precursor before initiating the ALD process [1]. Proper treatment, according to the deposition modifications, helps to achieve optimal deposition conditions and satisfactory results.

The first step: depicted in Fig. 2.1 (b), after the substrate has been deposited into the reactor chamber and deposition conditions, such as chamber pressure or substrate temperature, have been set in accordance with deposition recipe precursor A (first) is pumped into the chamber. The precursor exposure period is specified so that precursor could react with the substrate in a self-limiting manner [1]. ALD process is designed so that precursors are restricted to react with only available surface sites. As the reaction goes, active surface sites are depleted. When all of the surface bonds are occupied with the main precursor element, the reaction self-terminates, regardless of any excess precursor species that are present in the reactor [19]. Saturation is achieved, leaving reaction by-products, leftover precursor species and newly grown sub-monolayer, which is ready to react with co-reactant.

The second step: depicted in Fig. 2.1 (c), after saturation is reached, the reactor chamber is filled with residual precursor molecules and gaseous reaction by-products. The reactor is then purged with the inert gas carrier (usually Ar or N_2) and cleared of unnecessary elements [1]. Purge periods are adjusted accordingly with the chemical composition of the precursor. Sufficient purge periods are detrimental since they ensure the composition quality of the final product and prevent potential reactions of ensuing precursor with remaining precursor molecules or reaction by-products and subsequent contamination of deposited film.

The third step: depicted in Fig. 2.1 (d), precursor B (second) is pulsed into the chamber for a sufficient time to reach saturation and form the second sub-monolayer, finishing a single monolayer (ML). Excess precursor molecules and reaction by-products are left in the chamber. The third step mirrors the first one, accounting for the specifics of precursor B.

The fourth step: depicted in Fig. 2.1 (e), a second purge is initiated. Reaction by-products and precursor are purged from the reactor chamber, making it ready for the next cycle. A combination of one pulse period with the consequent purge period is called a half-cycle. Cycles are repeated until the desired thickness of the film is achieved, as shown in Fig. 2.1 (f). The incremental change achieved by the end of the cycle is used as a characteristic called growth-per-cycle or GPC [2]. Linear growth or constant GPC is desired and can be demonstrated in a steady regime of ALD. GPC depends on individual processes and can change throughout the whole deposition [19].

2.2 Characteristics and conditions of ALD process

Various characteristics such as GPC, temperature window, and time periods can be used to characterize a specific ALD process. Unique and advantageous properties of ALD are exhibited only when various depositions conditions are followed. Besides that, the variables of a specific ALD reactor and the specific process should be considered to optimize the deposition.

2.2.1 Growth rate

One of the main characteristics, which is used to describe the deposition process practically, is the incremental growth of deposited film per cycle or, as mentioned previously,

growth-per-cycle. As the reaction between precursor and surface substrate reaches saturation, the film growth stops increasing and starts to plateau at a steady number [20]. This self-limitation is what allows to calculate a typical growth per cycle.

GPC is usually calculated as the final thickness of deposited film against the total number of cycles [19]. Calculations can be done both in-situ and ex-situ. Ex-situ calculations are done using methods such as single wavelength ellipsometry measurement that uses data from multiple depositions. In contrast, in-situ measurement, which provides more practicality, can be done in real-time during a single deposition via spectral ellipsometry [19].

Ideally, constant GPC is desired. It is ensured through that an equal number of surface sites are consumed and regenerated in a deposition cycle, but this condition is challenging to achieve [19]. Various factors such as material densities, the relative size of atoms, crystallinity and interatomic planes, substrate material, and deposition temperature exert influence on the film growth [20]. Also, the calculation of GPC in multilayer systems may not be as simple as a sum of several independent processes.

2.2.2 Temperature

Deposition temperature is another essential characteristic used to describe a particular process. Temperature determines the availability of precursors and heavily affects the crystallinity of all inorganic films deposited by ALD [21].

The temperature range within which the deposition exhibits self-limiting nature is called temperature window [1] and it is specific for a particular process. An idealized window scheme of the ALD process with undesired effects is shown in Fig. 2.2.

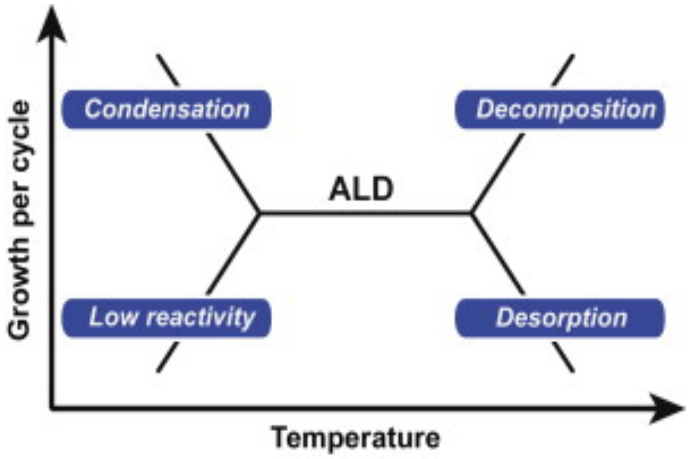

Figure 2.2. Idealized ALD window scheme [2]

GPC is not affected by the temperature variations inside this window, but if the temperature values reach outside of the specified limits, several undesirable effects may hinder the properties of the ALD process [2]. GPC may suffer from temperatures both over and under the temperature window. At lower temperatures, molecules may show lower reaction kinetics, preventing the occurrence of complete reactions and saturation, hindering the resulting GPC [1]. GPC may also be decreased due to either desorption or etching of grown film at higher temperatures [2]. Temperatures over the specified window may also lead to the decomposition of precursor species, which results in the incorporation of undesired CVD components into the deposited film and an increased growth rate. Increased GPC may also occur at lower temperatures, which happens due to the condensation of reactants on the surfaces. Condensation also decreases purge effectiveness, causing excessive contamination of the deposited film [2].

The substrate temperature is another significant characteristic that is important for deposition. It determines the thermodynamic feasibility and kinetics of the undergoing ALD surface reactions [19]. The substrate temperature is usually restricted by the upper limit, above which deposition loses its self-limiting nature. Reactor design and thermal stability of the substrate are additional factors that must be counted when determining optimal substrate temperature. Other temperature parameters for a specific ALD process may affect deposition results. For example, the growth of ZrN using PEALD is affected by the valve temperatures [22].

2.2.3 Time periods

Durations of various deposition steps significantly affect the properties of the ALD fabricated film. Sufficiently long reactant exposures and reactor purges may help GPC to reach a constant value, which then will not be affected either by the extended exposure time or by the increased purges period [19]. Short purge periods lead to the presence of excess precursor and reaction byproducts in the reactor chamber during subsequent precursor exposure step, thus possibly leading to contamination of grown film with CVD components or unnecessary by-products [2].

Since ALD is less dependent on the molecular flux due to the self-limiting nature of reactions, a difference in flux within different areas of complex 3D topologies may be compensated by the increase in the exposure time to achieve conformality [2]. Limited by gas phase diffusion, precursor and reactant transport in high aspect ratio features of 3D topologies requires an increase in pulse periods of both reactants to attain conformality and uniformity within deep features [19]. Computational simulations, such as Monte Carlo-based simulations, are used to predict proper pulse and purge periods better for specific ALD processes [5].

The deposition rate is a temporal characteristic of an ALD process. It is described by a number of layers that are deposited in a set period of time. Most ALD deposition rates are of order 100-300nm/h [23]. Deposition rate strongly depends on the reactor design and aspect ratio of a substrate. As mentioned previously, complicated non-planar high aspect ratio structures require longer pulse and purge periods to achieve conformality, increasing the overall deposition rate. Increasing the volume and surface area of the reactor chamber also increases purge and pulse time periods.

2.3 Advantages and shortcomings of ALD

ALD provides undeniable advantages, which stem from sequential self-saturating reactions of precursors with the surface. These advantages are unique to ALD and are achieved for the specified conditions dictated by the deposition recipe.

2.3.1 Thickness and composition control

Self-limiting nature of the ALD process, as well as the cyclic layer-by-layer deposition manner, allows for precise thickness control of the deposited film and composition tuning and simplifies the research into the mechanism of surface grafting and film growth [20]. In general, the thickness of a single layer of the film deposited during a cycle is less than $1\mathring{A}$ (Angstrom), with regard to a specific process [1].Consequently, the overall thickness of the deposited film can be adjusted at the atomic scale by controlling the number of repeated deposition cycles.

Composition tuning allows for the creation of complicated materials of more than two chemical elements. Incorporation of additional chemical elements can be done

by a variety of methods, from simply increasing the number of deposition steps, as a multistep process, to combining multiple ALD processes in a specific ratio. Additional elements are represented as an additional layer or as nanoparticles doping of the film. The combination of multiple ALD processes is known as supercycle, and it can be used to grow alloys or doped materials [2]. Supercycle consists of m repeated cycles of the first process and the subsequent n repeated cycles of the second process. Adjustment of the m:n ratio can play a detrimental role in defining material properties such as conductive behavior or optical properties in the case of zinc-tin-oxide deposition, which uses ALD processes for SnO_x and ZnO [1]. Fig. 2.3 depicts the scheme of various step combinations in the above-mentioned processes [2].

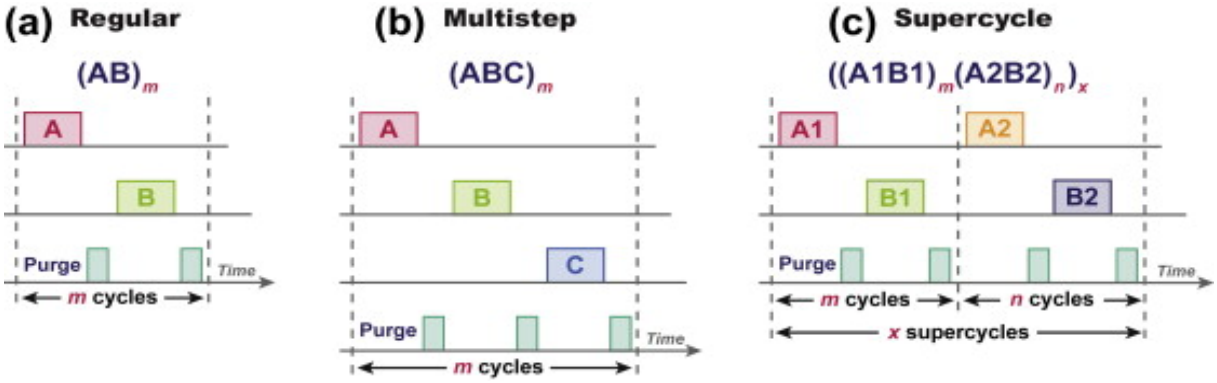

Figure 2.3. Schematic representation of steps in a) a regular ALD process, (b) a multistep process and (c) a supercycle [2].

It should be stated that for metal oxides, ALD processes thermal compatibility is required for successful deposition and that often ratio of cycles and ratio of the deposited layer does not have a linear relation [1]. This creates complications when designing supercycles.

There is a concern that atomic-scale thickness control may not always be guaranteed. Various kinetic and steric factors affect the actual thickness per growth cycle, making it less than 1 ML/cycle [5]. Thickness control may also be affected by growth delay or growth enhancement effects. Ideally, immediate linear GPC is desired for the ALD process; however, substrate material or its treatment may affect the growth rate at the beginning of the deposition, leading to an increased or decreased growth rate [2]. Another growth deviation that may decrease the GPC of the ALD for specific material systems is the formation of ”islands”, zones of increased initial growth [5]. The formation of ”islands” is usually observed for metal oxides but not restricted to them.

Considering the information mentioned above, the effects that cause growth deviation can be potentially beneficial at the same time. For example, ”island” formation can be used for controlled growth of islands or even nanoparticles [2]. Additionally, dependence on the starting properties of the wafer surface can be used, by appropriately altering deposition conditions and process, to create a modified ALD process, such as selective growth ALD [2].

2.3.2 High conformality and uniformity

High conformality and uniformity are the qualities that are usually sought after when choosing ALD as a primary deposition method. Conformality indicates an equal thickness of deposited film throughout the structure’s surface, and uniformity illustrates that film or coating is the same structurally and compositionally over the entire structure

surface. These qualities are attributed to the self-limiting nature of the ALD process. Conformality is a detrimental quality since emerging nano-scale devices are not only limited to planar structures but exhibit complicated 3D topologies. Fig. 2.4 (a) show an excellent conformality and step coverage of of PEALD grown TiO_2, Al_2O_3 and SiO_2 films in dense trenches. Each layer can be distinctively seen in the cross-sectional HAADF-STEM image Fig. 2.4 (a) and Fig. 2.4 (b) shows Energy Dispersive Spectroscopy (EDS) map, that shows each deposited elemnt.

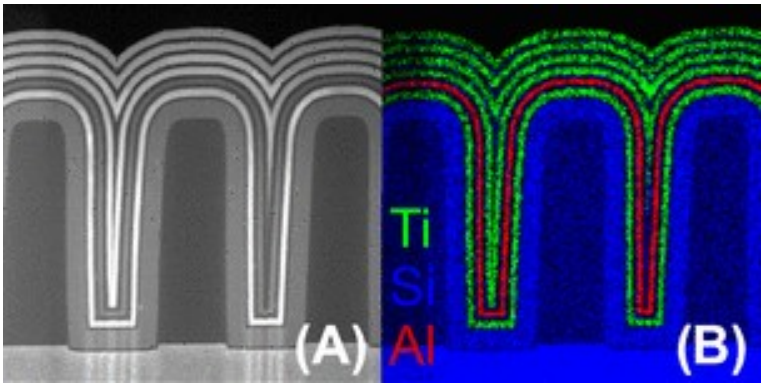

Figure 2.4. Cross-sectional HAADF-STEM image (a) and EDS map (b) of of a stack of alternating TiO_2 and SiO_2 layers and a single layer of Al2O3 [3].

To achieve high levels of conformality, deposition conditions should be fulfilled, and saturated absorption of precursors should occur over the entire surface of the structure. This condition may be easier to achieve on flat surfaces, whereas complex 3D high aspect ratio structures require a more complex approach to achieve high degrees of conformality. Complex structures, like trenches or holes, require saturated absorption of precursors both outside and inside of them [5]. While a flat surface saturation may be achieved at a certain amount of time, due to differences in conditions and deposition regimes, the degree of saturation over the complex 3D topologies may differ. Incomplete saturation reactions may occur deep inside holes or trenches, leading to a diminishing layer of thickness going from top to bottom and thus a poor level of conformality. The degree of saturation is determined by several factors, including molecular flux, adsorption or desorption probability, and surface diffusion [5].

As mentioned previously, an increase in exposure time may be a solution to improving conformality. Depending on the deposition regime, however, this condition may differ. For diffusion-limited growth, which occurs in very high aspect ratio structures or for high probability reactions, both exposure and purge periods should be largely extended to achieve saturation at the bottom of the trench [2]. This might not be the case for recombination-limited growth, which is typical for plasma or ozone co-reactants since the increase in exposure time might be impractical due to extensive exposure time necessary [2]. For reaction-limited growth, conformality may be achieved even without saturation conditions. Sticking probability is another factor that can be affected by modifying the surface in order to improve saturation [5]. It is necessary to use various mathematical models of step coverage of ALD to gain more insight into how deposition may be improved.

Various chemical side effects can diminish the conformality and uniformity of the deposited film, including decomposition, surface poisoning, etching, and process interactions [2]. Decomposition of precursor in the gas phase or on the substrate surface may lead to a CVD component, which increases non-uniformity. In particular, decomposition becomes an issue when an ALD process, designed for single-wafer equipment, is

applied without particular modification to batch production tools [2]. Surface poisoning and etching are usually the results of reaction by-products.

2.3.3 Low temperature deposition

ALD is vastly used for another unique and robust advantage: the possibility of deposition of high-quality films at relatively low temperatures, with rather low impurity levels, compared to CVD [5]. This is attributed to the ALD-specific quality, that surface reactions are complete. Substrate heating is needed to activate surface reactions with precursors [5]. A typical range of temperatures for the ALD process to achieve these properties is between 150°C and 400°C, which is lover compared to CVD. Several ALD processes of specific chemistry combinations have been deposited at temperatures under 100°C, even at room temperatures [20, 5]. For example, a so-called "golden standard" ALD process, deposition of Al_2O_3, which uses trimethylaluminum (TMA) and water, is possible at temperatures as low as 33°C [24]. Even though the film density was lower and hydrogen levels were higher in comparison to films deposited at 177°C, Al2O3 film had good electrical properties and a smooth surface. Other material compounds deposited at low temperature depositions include TiO_2, SiO_2, B_2O_3, CdS and VO_2 [20, 5].

ALD process for metal films requires reducers to clear the surface of the remaining ligands. Compared to the reactivity of oxidizers used on the deposition of metal oxides, the reactivity of reducers is lower [5]. Thus, in general, temperatures for deposition of metal thin films are higher in comparison with metal oxides, and a relatively small amount of depositions have been reported at temperatures under 100°C. For example, Cu has been deposited at 50°C using reactive H_2 plasma [25].

Whereas metal ALD requires higher deposition temperatures, deposition on polymer substrates requires low temperatures of the ALD process, in general below 150°C [5]. An exception can be a group of thermally robust polymer materials, which were studied for the deposition of diffusion barriers on low-κ dielectrics. The application of low-temperature ALD with heat-sensitive materials, such as most polymers and biomaterials, still requires further research.

Several modifications can be implemented to decrease ALD process temperatures further. In order to decrease the temperature, usually, the reactivity of precursors (co-reactant) should be increased. Less common approach is the utilization of catalysis. However, this can generally be done using energy-enhanced ALD processes, such as plasma-enhanced ALD [5]. PEALD has been successfully used to deposit a numerous compounds, including such prominent oxides Al_2O_3, TiO_2, and SiO_2. PEALD at room temperatures was used to deposit Al_2O_3 on heat-sensitive polymer and wool [5, 2].

2.3.4 Drawbacks

With all the benefits of ALD listed, it is also important to mention several drawbacks of this deposition type. In order for ALD to stay one of the most progressive deposition methods, which enables future generations of technologies, these shortcomings and limitations should be appropriately analyzed and addressed.

The ALD process generally suffers from slow deposition rates [1]. As mentioned previously, deposition rate depends on reactor dimensions and structure as well as accumulative purge and pulse time periods. Deposition of the film is done in a layer-by-layer manner. To achieve high conformality and uniformity in a single layer of complex non-planar structures, single step time periods are usually increased, thus decreasing

the cumulative deposition rate. Most ALD rates are on the order of 100-300 nm/h [1]. Spatial and other modifications of the ALD process are used to resolve this issue.

In order to minimize levels of contamination in fabricated film, ALD requires precursors and process gasses of ultra-high purity (usually in ppb trace levels) [19]. Maintaining high purity levels is expensive, thus increasing the overall cost of the deposition process. Since more fabricated devices approach the atomic scale of dimensions, the influence of the minor contamination levels may be crucial to their performance. It is necessary to study mechanisms of contamination in ALD films in order to reduce operational costs and improve the quality of produced films.

Another issue that ALD has is that the wasted portion of gaseous precursors is emitted into the environment [16]. For example, during reactions involving TMA, CH_4 (methane)is emitted, which is hazardous for both the environment and professionals operating the ALD equipment. Both inclusion of new chemistries with potentially less harmful precursors and improved evacuation methods of emission reduction or prevention should be investigated as an improvement to the ALD process.

2.4 Materials

The variety of materials deposited by the ALD process has been expanding over the last three decades. It includes but is not limited to nitrides, carbides, sulfides, selenides, tellurides, pure elements, and, being the most applied, oxides [21]. Fabrication of materials is mainly focused on producing crystalline and amorphous films. ALD process is most commonly applied for the deposition of binary materials, but pure elements and materials consisting of 3 or more compounds can be fabricated. The choice of chemical elements for the ALD is vast, but it is limited by the availability of reaction pathways as well as the choice of reactants that can facilitate the proper reaction pathway [1]. Besides that, reactants should fulfill a list of requirements, including

- Reactants must be volatile enough to stay in a gas or vapor phase at the temperatures lower than the ALD reaction [20];

- Reactants must react in a fast, irreversible, and saturating manner with sites on the surface;

- Reactants should have relatively high decomposition temperatures to stay intact during the storage and growth process; Thermal stability of reactant helps to reach saturation, preventing unnecessary further reactions [21];

- Reactants should not damage the growing material;

The variety of available chemical compounds involved in and deposited by ALD is illustrated as a table [4] in a Fig 2.5.

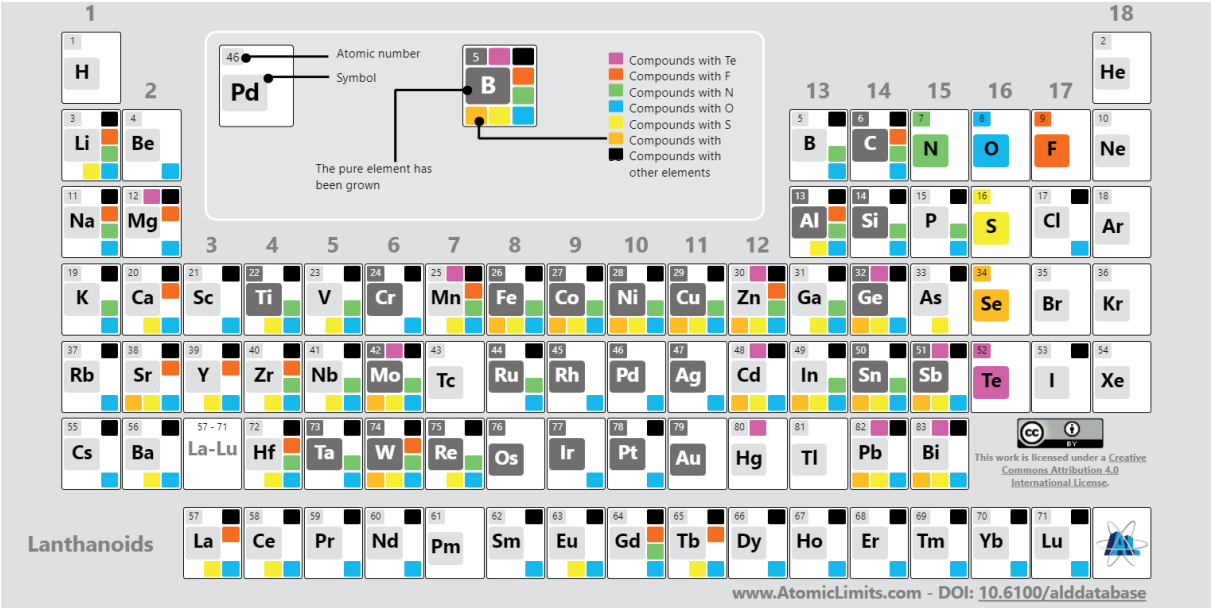

Figure 2.5. Table of the available materials and processes for the ALD [4].

It is essential to state that for many years majority of precursors that have been used for ALD were initially designed for CVD and metalorganic-CVD (MOCVD) [20]. Due to the ever-increasing requirements of the microelectronic industries, the deposition of older generations of reactants struggles to provide necessary lower temperatures and higher quality and growth rates with thermal ALD. Thus, further research into specially designed ALD precursors, which may take advantage of the unique qualities of the ALD process, is needed.

2.4.1 Precursors

The most commonly used type of precursors used in ALD are metal-based compounds. Metal reactants can be divided into two major categories according to their ligands: inorganic complexes such as metal halides and elemental metals and metal-organic complexes, with the most used being alkyls, amides, alkoxides, cyclopentadienyls, β-diketonates, silyls, phosphines, imides and amidinates, and their modifications [21, 1]. Mostly, ligands affect the reactivity of the precursor.

The categorization of precursors can further be expanded and done according to their elemental group. Many of the main group metals, transition metals, and lanthanides have seen usage with the ALD processes [2]. Group 4 metals oxides such as Ti, Zr, and Hf have been extensively used with the ALD process [20]. Transition metals and their derivatives have many vital applications in electronic industries. Noble metals Pt, Ru, and Os, are also used in the ALD process and are particularly interesting as films resistant to corrosion and oxidation. Fig. 2.6 shows an excellent conformal layer of Ru deposited by ALD [5].

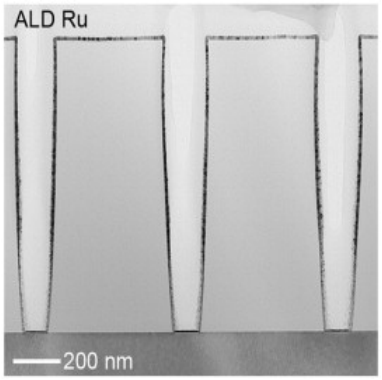

Figure 2.6. ALD layer of Ru in nano trenches [5].

Group 13 metals are one of the most established groups due to the deposition of Al with Al_2O_3 deposition as a golden standard of ALD process [20].

2.4.2 Co-reactants

The second reactant plays a vital role in what type of material is being deposited. Most commonly deposited materials are oxides, and this group has the most extensive choice of co-reactants. The most used co-reactants within oxides and other groups of materials are hydrates of non-metal elements: water H_2O, ammonia NH_3, hydrogen sulfides H_2S [21]. This group of reactants shows high stability and reactivity in vast temperature ranges.

The most commonly used oxygen source for the deposition is water H_2O, which can sustain higher deposition temperatures and is gentler than most oxides sources. However, H_2O has relatively low reactivity and may not be used to deposit precursors which are already less reactive at lower temperatures. It also may be problematic to purge water from the reactor because it strongly adsorbs to surfaces [2]. Other oxygen sources have been proposed to improve these shortcomings. H_2O_2 has been suggested as well instead of H_2O to improve reactivity in many depositions since it contains less stable O-O bond. Likewise, ozone O_3, which is one of the critical components of the energy enhanced ALD, is used to deposit oxides from less reactive compounds with bulkier ligands, which usually do not react with water [21].

2.5 Modifications of ALD

The relatively slow deposition rate and geometry of the default reactor may be a barrier between ALD and its implementation in the industrial fabrication process. Thus, specific modifications to the reactor and ALD process are required to accommodate various production methods and be natively integrated into the production line. Fig. 2.7 shows ALD reactor and process modifications which will be described below.

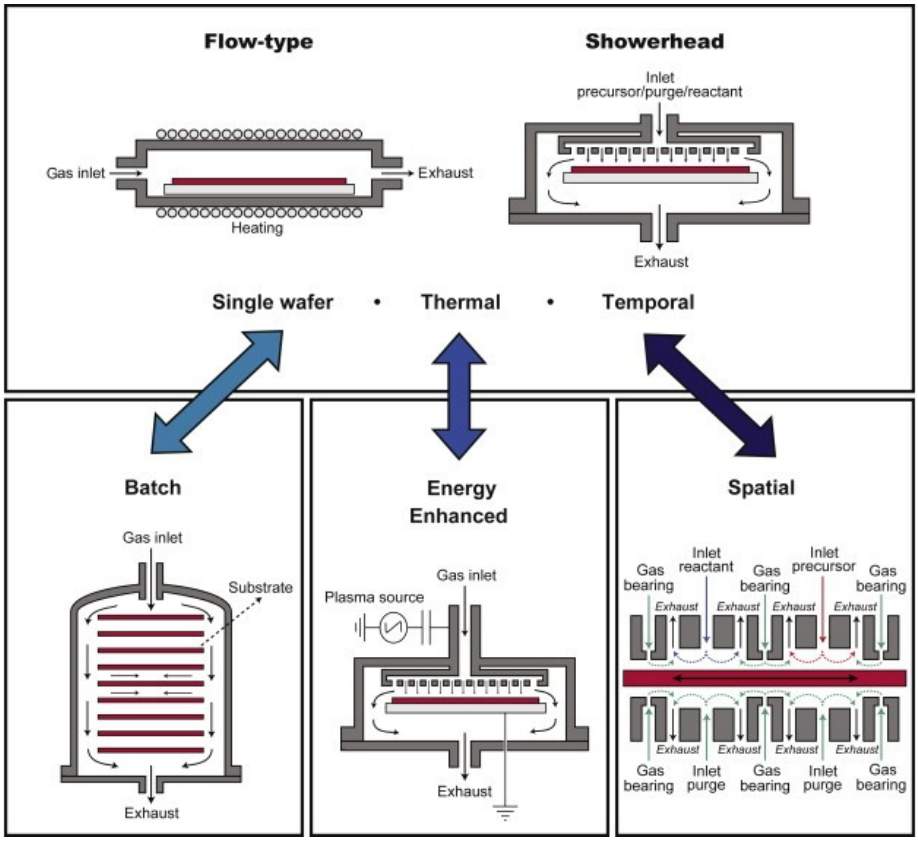

Figure 2.7. Modifications of ALD process [2].

2.5.1 Showerhead reactor

Unlike the flow-type reactor, shown in the upper-left part of Fig. 2.7, where usually precursor gases are carried by the inert gas and pass through the reactor, showerhead type reactor, depicted in the upper-right part of Fig. 2.7, uses a special nozzle that helps to evenly distribute precursors across the whole deposition surface [2]. Both flow-type and showerhead-type reactors use wall heating and substrate heating options.

2.5.2 Spatial ALD

As shown in the lower-right part of Fig. 2.7, modification of spatial ALD uses a very different approach to increase throughput. It could be stated that the spatial ALD process is based upon sequential thermal ALD. In spatial ALD concepts, steps of an ALD cycle are not separated in a time domain but conversely are separated in the spatial domain [2]. Exposure of precursors is not done in separate steps divided by purging periods, but rather their exposure occurs at different positions using different reaction zones separated by purging areas, which require high pressure and sufficient supply of the purge gasses [15]. Then, to periodically introduce substrate to different precursors, either the substrate itself or the deposition head is moved. As a result, throughput becomes dependent solely on the specifications of the reactor, such as volume or substrate load and reaction kinetics [15].

2.5.3 Batch ALD

Batch ALD, which can be seen in the lower-left part of Fig. 2.7, uses an extended and modified reactor that allows simultaneous deposition on multiple devices. Typically

a single processing load varies between 50 and 500 [2]. Increased reactor volume and a large number of wafers require alteration of the deposition process to achieve optimal results [15]. Due to the increased volume of the reactor, uniformity might slightly decrease, and, as previously mentioned, exposure and purge periods should be sufficiently increased. Conversely, overall high throughput is still achieved due to multiple simultaneous depositions.

2.5.4 PEALD reactor (Energy enhanced reactor)

Energy-enhanced ALD is a modification in which film growth is enhanced by adding extra energy to a co-reactant and converting them into highly reactive species [26]. The principle scheme is shown in the lower-middle part of Fig. 2.7. PEALD is a subcategory of energy-enhanced process, which provides such benefits as increased precursor availability, lower deposition temperatures, and increased GPC [26]. PEALD, as said in the name, uses plasma of the gas as a highly reactive species. Plasma consists of a mix of free-charged particles and other reactive atomic and molecular gas species [26]. Due to the short-term stability of highly reactive species, the generation of plasma should be done in situ or so that the whole deposition process could be done relatively close to the substrate [2]. O_2 plasma has been used to deposit oxide of rare earth materials such as RE, Pm, EU, and H_2 plasma in reactions with carbon-containing precursors [20]. Pure metals can also be deposited using H_2 or O_2 plasma, which leave a pure ligand-free metal surface [2]. It should be noted that for some chemistry, highly reactive co-reactants may damage the surface and thus decrease uniformity.

Chapter 3
Application in photovoltaic devices

Due to a continuous trend of miniaturization in various electronic applications, ALD film production has found itself in the applications spawning over numerous industries, starting from semiconductors and electronics up to medical devices [16, 1]. Thin films may be applied in various environmental applications, and they can be used to improve the efficiency of water filtration units or enhance the wastewater treatment process. The application of ALD in semiconductors industries has enabled further miniaturization of the newly developed devices. ALD may enable the future development of flexible electronics due to its ability to deposit on heat-sensitive substrates like plastics. ALD has already played an essential role in the successful integration of high-κ dielectrics in semiconductor devices

In particular, ALD has been irreplaceable in the production and evolution of energy storage and harvesting devices, such as photovoltaic devices or solar panels. A typical solar cell can be described as a semiconductor device made of single crystals, crystalline (c-), and amorphous (a-) semiconductors. The solar cell has various layers which play a particular role in converting light into electrical energy. In general, conversion is done by absorbing light of various wavelengths and creating of electron-hole pair in the crystal. Oppositely charged carriers should be separated and accumulated on opposite sides of solar cells, essentially making solar cells a battery, a source of electrical energy. If electrodes are connected on respective sides, current can flow between them [27]. The creation of regions within the solar cell with increased concentration of particular carrier, by adding dopants with appropriate bandgap work function and conductivity, separates opposite charges and prevents their recombination [11]. A vital role in that play junctions between various regions or layers, a so-called p-n junction is one of them and various layers themselves [27]. Higher power conversion efficiencies and low losses of PV devices are facilitated by precisely tuned interfaces since their composition, geometry, and qualities affect the junction and behavior of charge carriers within the cell. Various interface engineering techniques are used to modify interfaces, and ALD can be considered one of them.

3.1 Surface passivation layer for c-Si and a protective layer for quantum dot solar cell

The surface passivation layer may be seen as the outer layer of the main bulk of the solar cell. Its purpose is to trap photogenerated electrons and holes and stop them from unwanted recombination at the surface [11]. A layer of dielectric material may be used to passivate surface defects. An effective charge carrier confinement is achieved via a combination of chemical passivation, doping, and stimulation of work-function difference at the surface.

Currently, the c-Si solar cell industry's goal is to reduce the cost per watt peak, which can be done by reducing the cell thickness and improving efficiency [15]. Effective surface passivation layers can reduce recombination losses at the interface of a solar cell,

making that goal more feasible. Besides improving passivation properties, dielectric surface passivation can contribute to the reduction of optical losses by increasing internal reflection [15]. Metal oxides, including aluminum oxide Al_2O_3, hafnium oxide HfO_2, titanium oxide TiO_2 as well as various silicone compounds, have been tested to passivate c-Si surfaces [28]. ALD grown dielectric layer can provide the required thinness and improved uniformity. Out of the previously mentioned compounds, using the ALD method, Al_2O_3 and HfO_2 have been widely grown and studied. Al_2O_3, the most successfully used ALD passivation material for Si solar cells, has consistently intrinsic negative fixed charge density [7]. At the same time, HfO_2 may possess either positive or negative fixed charge depending on the precursors or deposition conditions of ALD. For example, a negative fixed charge was exhibited for the ALD process with hafnium (IV) chloride ($HfCl_4$) and H_2O as the precursors, and positive charge density was observed for tetrakis(diethylamido)hafnium (TDEAH) and water [29]. As for ALD Al_2O_3 film, high-quality passivation for both p-type and lightly doped n-type c-Si was achieved with surface recombination velocities (SRVs) below $10cm.s^{-1}$ for both types of Si [28]. These results were attributed to a combination of chemical passivation and "field-effect passivation." Other metal oxides, such as Ga_2O_3, Ta_2O_5 and PO_x have been used to synthesize passivation layers for c-Si solar cells [7].

Inorganic quantum dots (QDs) are nanostructured materials, used in the third generation of PV technology, that primarily influence the main advantages of third-generation solar cells, such as low component cost, high optical absorption, and improved charge carrier collection [30]. QDs solar cells are attractive as well because of their fascinating semiconductor characteristics: bandgap tunability, size-dependent band energetics, high absorption coefficients, the possibility of multiple exciton generation (MEG) and multiple exciton collection (MEC) [7], which can be adjusted with their sizes. QDs are inherently metastable and undergo chemical and physical changes because of their high surface-to-volume ratio.A layer of high bandgap transition metal oxide (TMO) coating deposited by a low-temperature ALD can protect QDs from various physicochemical changes (oxidation, Ostwald ripening, surface diffusion, agglomeration, and coalescence) [7]. This protective layer also acts as an infiltration layer enhancing conductivity by filling the gaps in the nanocrystalline fim. As a result, conductivity and charge carrier mobility are advantageously modified, which can be demonstrated by infilling the ZnO layer, done by ALD, into CdSE QDs-based films [31]. Due to the ability of ALD to deposit conformal films deep into trenches of complicated 3D structures, it has emerged as an effective method to tune the properties of close-packed nanocrystal assemblies. ALD is an optimal deposition method to uniformly coat QDs to improve their stability and performance.

3.2 Carrier selective contacts for c-Si solar cells and transport layer for OPV

Charge carriers, electrons and holes should be separately transported to the two metallic terminals of a solar cell to deliver their energy to the external load [11]. However, this becomes problematic due to various undesired effects in the regions of solar cells, such as nonradiative recombination, decreased carrier mobility, and parasitic light absorption that increases minority carrier conductivity and decreases contact selectivity [32]. Thus asymmetric conductivity for electrons and holes in different regions of a solar cell and heterojunction carrier selective contacts should be employed [7]. Production of an effective carrier selective contact is an optimization process since a thicker layer helps

to improve contact selectivity and reduce contact recombination while a thinner layer minimizes extraction losses and parasitic absorption [32]. ALD can play a crucial role in producing an optimized selective contact layer due to its precise control capabilities and other intrinsic benefits.

High-quality selective contacts can improve the efficiency of c-Si solar cells. TMOs can be utilized for that purpose due to their superior properties: significantly higher optical transparency than a-Si, lower deposition temperatures than poly-Si, and do not suffer from Auger recombination like highly doped Si contacts [7]. Typically, TMO carrier selective contacts require a thickness of less than 5nm, and thus ALD process for TMOs can be naturally employed to produce high conformality thin films.

Molybdenum oxide MoO_x might be a rather promising film grown by ALD that can be used as a hole selective contact. Currently, the method used to grow that film is thermal evaporation. It was shown that MoO_x film grown by thermal evaporation has slightly higher band-bending values of 0.8eV in n-type Si than the MoO_x film grown by PEALD (approx. 0.7eV) [7]. Optimization of deposition conditions, post-deposition treatment of the film as well as various enhancement methods of the growth process, such as Density Functional Theory (DFT) calculations, can help to overcome this difference and improve the qualities o MoO_x ALD contacts, leaving the significant potential for ALD in future devices. Other ALD-grown films can also benefit from DFT calculations. For example, DFT calculations have helped to determine how to alter ALD grown NiO_x film intrinsic diode properties on p-type Si [7, 33]. Using ALD supercycle process, Zn dopants were incorporated into NiO_x and the grown 3.4nm $Zn_xNi_{1-x}O$ film has demonstrated hole selectivity on p-type Si, and minimum contact resistivity of 21.5 $m\Omega \cdot cm^2$ was shown for a 0.62 concentration of Zn and annealing at 200°C ratio [33], thus increasing the number of ALD applications for hole selective contacts.

As for electron selective contacts, ALD films are represented by TiO_x. Ultrathin TiO_x film was grown using thermal ALD procedure and was used as an electron selective contact on n-type c-Si. The TiO_2 film of 4.5nm thickness had both good passivation qualities and relatively low contact resistivity at the TiO_x/Si heterojunction of 0.25 Ω cm^2, which allowed to fabricate a solar cell with an efficiency of 20.50% [6]. The structural scheme of such an n-type Si heterojunction solar cell is shown in Fig. 3.1.

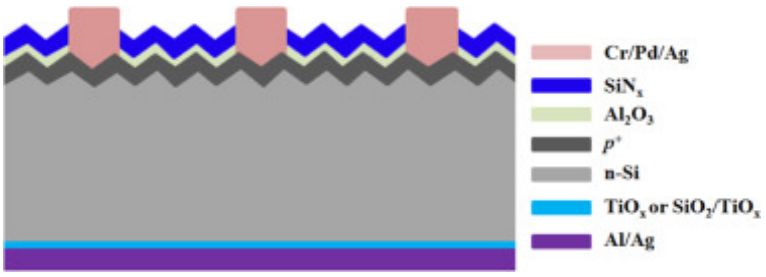

Figure 3.1. The schematic structure of n-type silicon heterojunction solar cell with TiO_x-based electron-selective contact at the rear side [6].

Other ALD films of TaO_x and Nb_2O5 were also successfully implemented as an electron selective contact improving overall PV device qualities [7].

In comparison with inorganic counterparts, organic photovoltaic (OPV) devices possess the advantages of low fabrication costs and light-weight, semitransparency, a myriad of organic materials, and flexible active layers that allow to integrate them into various flexible devices [34]. The layered structure of OPVs includes an electrode and transparent electrode, which is usually indium tin oxide (ITO), that confine the ab-

sorber layer and carrier selective transport layer. Normal and inverse structures of OPV solar cells can be seen in Fig. 3.2.

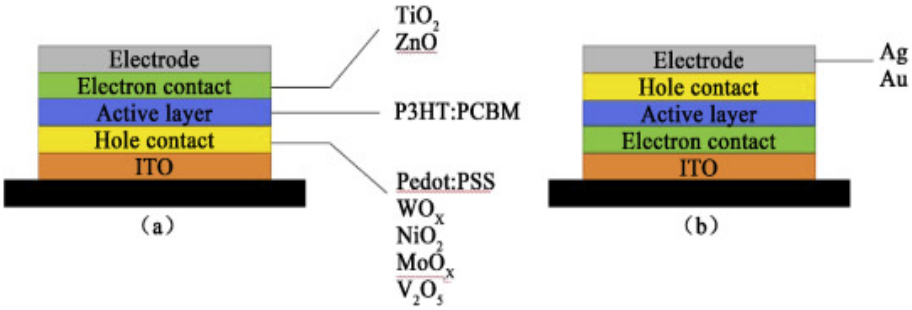

Figure 3.2. (a) A normal structure of OPV solar cell, (b) an inverse structure of OPV solar cell [7].

Various plastic polymer bulk heterojunctions (BHJ) are used in current OPV devices. Traditionally poly (3,4-ethylenedioxythiophene):poly (styrenesulfonate) (PEDOT:PSS) has been used as a hole transport layer, but the interface with ITO has caused issues because of PEDOT:PSS acidity [7]. Thus, a replacement in the face of metal oxides has attracted attention as an alternative carrier transport layer. NiO film, with good stability and electrical/optical properties, was deposited using thermal ALD and acted as a hole transporting layer [35]. A layer of 4nm of NiO was found to be optimal, replacing PEDOT:PSS and resulting in comparable energy conversion efficiency of 3.4%. At the same time, both ZnO and TiO_2 are deposited by ALD and can be used as an electron transporting layer in OPV [7]. ZnO layer of 2nm thickness deposited via ALD onto a ZnO ripple structure in an OPV resulted in the enhancement of the initial performance of the solar cell and the stability of cell performance. ALD process decreased the number of defects of ZnO and increased resistance toward surface defect formation [7].

3.3 Buffer layer and absorber layer for thin film solar cells

The buffer layer serves the function of optimizing device performance by maximizing light transmission into the solar cell and increasing the collection and extraction of charge carriers [7]. Buffer layers are commonly employed to improve various properties of thin-film solar cells. Thin-film solar cells are considered a promising alternative for c-Si solar cells due to several benefits: reduced energy requirement and material consumption and theoretical higher efficiency numbers, and new applications [7]. For chalcopyrite thin-film solar cells (CIGS) based on $Cu(In,Ga)Se_2$ and for Cu_2ZnSnS_4 (CZTS) solar cells, CdS buffer layer is commonly used [15]. The buffer layer, a heterojunction, ensures good interfacial properties between the absorber layer and a layer of transparent conductive oxide (TCO). Proper bandgap alignment with both layers is needed to increase the depletion layer [7]. The absence of the layer causes poor efficiency and low open-circuit voltage. In addition to affecting the cell's open-circuit voltage, it is commonly reported that layers affect stress-induced degradation and transient phenomena in CdTe and $CuInSe_2$ based solar cells [36]. However, the use of the CdS in the thin-film solar cells raises a number of concerns: Cd is a toxic and carcinogenic element [37] with a relatively low bandgap, and deposition of the CdS layer is usually done using the standard technique, the chemical bath deposition (CBD), which is the sole liquid phase in the fabrication process of CIGS [15]. CBD as a process provides

poor conformity that leads to cracks and pin-holes, which compromise stability and the performance of the deice [7]. ALD can serve as an effective alternative. ALD is a dry vacuum process, which can be incorporated easily into the production process, and works with numerous alternatives of Cd for CIGS and CZTS solar cells, and provides excellent control over the layer composition.

Some ALD films have been studied as an alternative buffer layer for thin-film solar cells, including In_2S_3, ZnO and its modifications, which have shown relatively favorable results [7]. The power conversion efficiency of 12.1% was achieved for CIGS Cd-free solar cells, with ALD ZnO film and without antireflective coating [38]. Further efficiency improvement was achieved after introduction of dopants. For example, Zinc-tin-Oxide ($Zn_{1-x}Sn_xO_y$) was deposited via ALD in a CIGS solar cell with an intrinsic ZnO to achieve an efficiency of 18.0%, which is comparable to Cd buffer layer [8]. One such layer produced in 2000 cycles can be seen in Fig. 3.3.

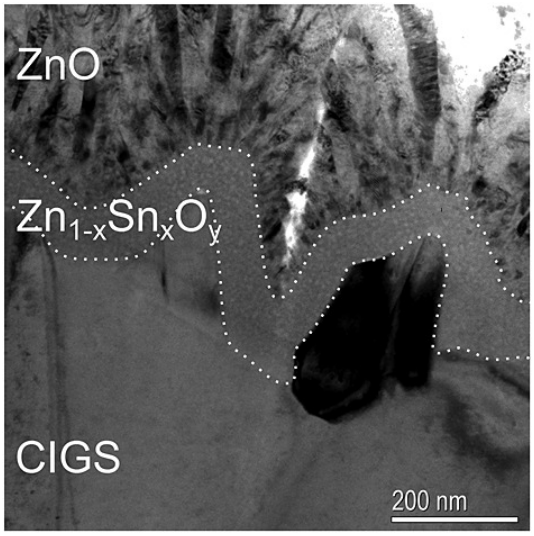

Figure 3.3. TEM image for the 2000-cycle thick $Zn_{1-x}Sn_xO_y$ buffer layer on Cu(In,Ga)Se_2 [8].

Utilization of ALD $Zn_{1-x}Sn_xO$ as a buffer layer provided flexibility to tune composition, by adjusting pulses of ALD, in order to identify the most optimal bandgap alignment with the absorber layer as well as sufficiently high bandgap to minimize optical losses [7]. Other buffer layers deposited via ALD, such as zinc-magnesium-oxide $Zn_{1-x}OMg_xO$ or zinc oxysulfide Zn(O,S), have been studied as the alternatives. An efficiency of 18.1% was achieved for CIGS solar cell with a 100nm ALD $Zn_0.8Mg_0.2O$ buffer layer deposited at 120°.

A combination of ZnO and Mg can also be utilized as an alternative window (second buffer layer) in thin-film solar cells. Sputtered intrinsic ZnO layer is commonly used as a window layer in CIGS and CZTS solar cells to increase shunt resistance by blocking pinholes, cracks, and voids [7]. However, a (Zn, Mg)O was proposed due to the wider bandgap and the possibility of adjusting the bandgap alignment by controlling the Zn:Mg ratio [39]. Since sputtering can possibly cause damage to the interface, it is also desired to replace sputtering with soft deposition techniques such as ALD, which can contribute to a higher film quality [7]. ALD film of (Zn,Mg)O was deposited as a window layer in a CIGS solar cell, with Zn(O,S,OH) acting as a first buffer layer. This combination resulted in the efficiency of 22% for the Cd-free buffer layer [39]. Zn_xTi_yO film produced by ALD has also been used as a window layer for CIGS solar cells, reducing the thickness of the CdS layer[40]. The composition control ability of

ALD was used to optimize the ratio of Zn and Ti in the window layer, thus achieving 20.8% efficiency.

The function of the absorber layer is, by absorbing light, to generate electron-hole pairs using donors and acceptors [41]. These photogenerated free charge carriers diffuse and drift under the influence of an electric field toward the respective transporting layer. For thin-film solar cells, including CIGS and CZTS CdTe, a search for an alternative absorber layer and an efficient fabrication process has also become a significant call. Utilization of toxic Cd and scarce materials such as Te, In Ga becomes an obstacle to fully implementing a large-scale production process [7]. A number of alternative absorbers that have been deposited via ALD require modifications to have characteristics on par with conventional materials used as thin-film absorber layer [7]. Precise layer modification at the nanoscale, which can be done using ALD, can improve the efficiency of the alternative absorber layers by modifying structural, optical, and electrical properties.

Absorber layers of Cu_xS, Sb_2S_3, $CuSb_2S$, and Cu_2ZnSnS_4 have been deposited via ALD process [7]. The ALD film of p-type Cu_xS was deposited on n-type TiO_2 and formed a high-quality p-n junction [7]. Precise control of deposition conditions of ALD, such as composition ratio, allows for tuning crystalline phase and stoichiometry. In the case of Sb_2S_3, the ALD process provided benefits of uniformity and decreased levels of oxygen impurities in comparison with the conventional CBD process, which resulted in the enhanced power conversion efficiencies from 2.17% for CBD to 5.77% for ALD [9]. The difference in precision of ALD grown layer and CBD grown layer can be seen in Fig. 3.4

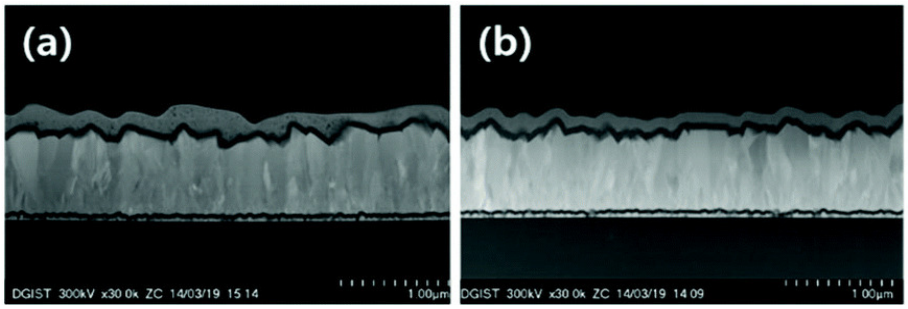

Figure 3.4. Cross-section of TEM image of (a) Sb_2S_3 CBD grwon layer of (90nm ± 30nm) thickness and (b) Sb_2S_3 ALD grwon layer of (90nm ± 6nm) thickness [9].

3.4 Encapsulation of CIGS and OPVs and growth of 2D materials

CIGS and OPVs require protection against moisture, various gases, and oxygen from the ambient [15]. Robust, transparent, and flexible materials are required for that task. ALD is a cable of low-temperature deposition of inorganic films with high uniformity, virtually pin-hole free. Encapsulation layer of 55nm Al_2O_3 deposited by ALD on top of CIGS solar cells provided excellent moisture permeation protection [42]. In the aging studies (>1000h) at 85°C/85% humidity, protection provided by the Al_2O_3 ALD layer was comparable with the glass. As for OPVs, ALD supercycle was used to deposit combined Al_2O_3/HfO_2, which has prevented O_2/H_2O-induced degradation and increased stability of the solar cell [10]. Encapsulation also provided an annealing step that helped achieve a power conversion efficiency of 3.66%. SEM images (c) and (d)

in Fig. 3.5 demonstrate how deposited Al_2O_3/HfO_2 laminate was virtually unchanged after storage for 200h in an environment with 28°C and 60% humidity, whereas two other films in (a) and (b), and (e) and (f) undergone some form of degradation [10].

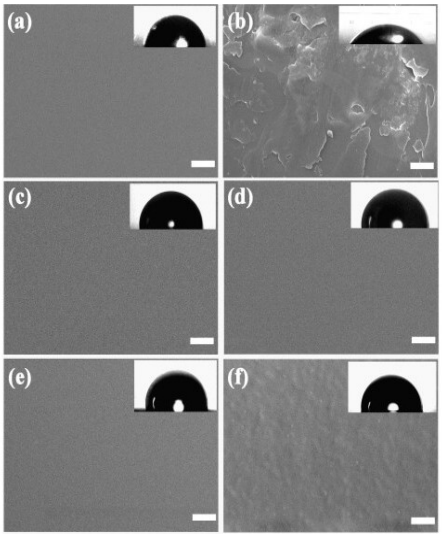

Figure 3.5. SEM images and water contact angles (inset) of ALD films deposited on the solar cells, before and after storage in air at 28°C with 60% relative humidity: (a) after deposition Al_2O_3, (b) Al_2O_3 after storage, (c) after deposition Al2O3/HfO2, (d) Al2O3/HfO2 after storage, (e) after deposition two-layer Al2O3/HfO2 and (f) two-layer Al2O3/HfO2 after storage. The scale bars in the SEM images are 1 μm [10].

ALD can be used to grow graphene and other 2D materials. 2D materials are considered coatings or films that have two dimensions outside of the nanoscale, a single atomic sheet of material restricted to one plane [43]. Graphene can be used as both charge injection and collection electrodes to alleviate problematic carrier recombination process in polymer solar cells(PSCs) [7]. CVD is the mechanism of graphene growth, which involves diffusion of the precursor into the Cu/Ni substrate to its saturation limits at high temperatures, around 1000°C, which is then followed by process of controlled cooling [44]. A monolayer of graphene is produced as a result of precipitation, which requires precise control of the cooling process. ALD can potentially substitute this highly meticulous process since it was reported that using remote PEALD at temperatures as low as 400°C, a high-quality crystalline graphene monolayer was produced [45]. Even though graphene hinders the growth of materials on top of it, ALD has successfully been used to deposit Al_2O_3 and TiO_2 [7]. It is also possible to grow graphene on various semiconductors, extending several potential applications in photovoltaic devices. Besides graphene, metal oxides and chalcogenides such as MoS_2, WSe_2, BN, MnO_2, $NbSe_2$ and Bi_2S_3 can also be grown as 2D materials [46]. Considering low growth rate and monolayer control, ALD can be used to grow various 2D materials and deposit layers onto 2D materials without degradation of the original properties of 2D materials [47]. 2D materials, due to their physical dimensions, and increased surface-to-volume ratio, exhibit unique properties which their bulk counterparts do not possess [48]. As ALD is established in the fabrication process of solar cells, 2D materials can be easily integrated into various photovoltaic devices. Unique properties of 2D materials can be taken advantage of to make more efficient, lightweight, and flexible solar cells.

Chapter 4
Choice of the dielectric material to enhance photovoltaic devices

It was decided to deposit a layer of Al_2O_3 using thermal ALD process onto textured Si wafer, for the purpose of enhancing properties of the Si based solar cell.

4.1 Silicon wafer

Silicon wafer-based solar cells have demonstrated significant technical and economic growth in the past decade [28]. To further advance the growth and deployment of this technology, possibilities to increase power conversion efficiencies and reduce production costs are researched.

Energy harvesting in the silicon solar cell is done by absorbing photons with energies above the silicon bandgap and generating electron-hole pairs and their consequent storage as a source of energy [49]. Formed charge carriers should reach respective selective contacts however, this may be prevented by recombination. In silicone, which features an indirect bandgap, recombination occurs due to defects in silicon bulk or at the silicone interface [49]. Recombination losses in various areas should be decreased to improve efficiencies. In PV fabrication, high power conversion rates are usually achieved by thinning Si solar cell wafers [49]. The production of silicon has significantly improved in the past decade, both the quality and cost efficiency [28]. High quality meant fewer impurities and defects in the grown bulk of the Si. As a result, recombination caused by the high defect density at the silicone surface started to play a significant role in decreasing the performance of PV devices. Passivation of silicon surfaces is paramount to achieving high power energy conversion rates. Deposition of dielectric surface passivation layer onto the silicon surface can significantly help to reduce unwanted recombination losses. Effective surface passivation prevents recombination at the surface, confining photogenerated charge carriers in the bulk of the Si cell and increases their number and electrochemical energy [11].

4.2 Surface Texturing

Texturing is essential for the optimization of power conversion of Si solar cells. Textured surfaces reduce the reflection of incoming photons and increase the mean path length of a ray of light within the solar cell [49]. It should be noted that recombination at the textured surfaces is generally higher than at surfaces of their flat counterparts [28]. This increase can be attributed to the increase in the overall surface area. In the case of monocrystalline silicon, which uses random pyramidal morphology, the increase is approximately 73% in comparison with the flat Si 100 surface [28]. Another reason for recombination increase is that, generally, the face of pyramids is a 111 surface and a larger number of dangling bonds concentrates at a 111 surface. Also, a higher concentration of surface defects in a textured surface is caused by mechanical stress in

the dielectric/Si interface [28]. These considerations should be taken into account while calculating relevant characterization parameters.

4.3 Passivation

The surfaces in a solar cell form an abrupt discontinuity in the semiconductor crystal lattice [28]. This discontinuity results in the disruption of the band structure and the formation of a semi-continuum of energy states at the bandgap. These states correspond to unterminated or strained bonds, known as dangling surface bonds [28]. Recombination arbitrated by bandgap states can be described using the Shockley-Read-Hall theory, that applied to a continuum of surface states however, for semiconductor surfaces, a relatively good estimation can be done by approximating the recombination activity of interface states of all energies into a concentration D_{it} of states at single energy in the middle of the bandgap, or know as the density of interface defects [28, 11]. The states at this energy have both electron recombination velocity and hole capture velocities, and taking into account these velocities a total recombination at the surface can be characterized by the effective surface recombination velocity S_{eff} (SRV). However S_{eff} can also be effectively calculated using formula

$$S_{eff} = \sqrt{D(1/\tau_s)}\tan(W/2\sqrt{1/D(1/\tau_s)}),$$

where τ_s is surface life time, W is width of the specimen and D is the ambipolar carrier diffusion coefficient [28]. Lower SRVs indicate higher quality of passivation and increased PV device performance. Other characteristics used to describe the quality of passivation of the deposited films are surface saturation current J_{0e} and implied open-circuit voltage $i\,V_{oc}$ [28].

Reduction of the recombination rate can be achieved through multiple means. First, completion of dangling surface bonds [11], by using dielectric coating or atomic species, can result in fewer available states or lower capture probability [28]. These effects result in the interface states hole and electron capture rate reduction. This reduction is commonly known as chemical passivation. Usually, atomic species of hydrogen are used to decrease the number of D_{it} and, as a result, recombination rate, however, a particular amount of D_{it} still remains after the treatment [11]. The presence of hydrogen has been detected in all high-quality passivation films.Overall, coating of the Si surface with a layer of dielectric helps to cover surface defects states, negating recombination caused by the latter. The second approach is based upon that the recombination rate is dependent on a ratio of the concentration of electrons and holes [28]. Recombination rate is fixed for constant p_s/n_s carrier concentration ratio in a steady-state conditions. Thus, reducing the recombination rate can be achieved by reducing the relative concentration of the particular charge carrier available at the surface and thus changing the ratio at the surface. Normally, the bulk majority carriers are responsible for the current flow in the semiconductor, whereas the minority carriers at the surface determine the rate of the recombination.The creation of imbalance where the majority carrier's concentration is higher than the minority carrier concentration helps to reduce surface recombination. Two strategies can achieve this imbalance. Firstly, in-diffusion of a high concentration of required dopants near-surface can be done [11]. Secondly, modification of concentration via an electric field, which is commonly known as "field-effect passivation," can be implemented [28]. The electric field is created by a fixed charge density of Q_f in the dielectric layer, which creates a mirror charge in the surface region of the silicon. In

the absence of external stimulants, the established electric field and the associated charge distribution near the surface are at the equilibrium [28]. Rather than repelling and decreasing the number of minority charge carriers at the surface, the electric field modifies the surface carrier concentration and attracts a large number of carriers, which in regimes of heavy accumulation and inversion, leads to the desired imbalance between the majority and minority carriers and a decrease in recombination rates upon carrier excitation [28, 11]. The recombination rate reduction is achieved via a spatial change in the carrier concentration near the surface, which is induced by the electric field. Some materials exhibit close to contact or in contact with the silicon a particular charge distribution, which can be seen in a Fig. 4.1. Understanding the difference between chemical passivation and field-effect passivation can provide further insight into the passivation mechanism and help to improve the passivation quality of deposited films.

4.4 Passivation layers for Si wafers

As a surface passivation layer for Si solar cells, several silicon-containing compounds have been used, including amorphous silicon (Si:H), silicon oxide (SiO_2), and silicon nitride (SiN_x) [28]. Thermally grown silicon dioxide, which effectively covers surface defects, requires an expensive and time-consuming process, which is conducted at temperatures above 1000° and is not easily integrable in various solar cell fabrication process [49]. PECVD fabricated silicon nitride does not face previously mentioned issues since deposition is usually done at temperatures around 400°C, and it has become the most widespread passivation layer for silicon solar cells [28, 11]. However, SiN_x contains positive charge carriers and deems to be inapplicable for the passivation of p-type doped silicon. Due to the availability of positive charge carriers and the near surface damage caused by the plasma deposition process, a reduced surface passivation quality is provoked, thus reducing the power conversion efficiencies of the PV device [49]. The presence of positive charge density also increases the concentration of electrons at the surface of the p-type silicon and reduces the passivation quality of p^+-type emitters of the n-type silicon-based solar cells. Many efficient architectures require high-quality passivation on the p-type silicon [28].

4.5 Al_2O_3

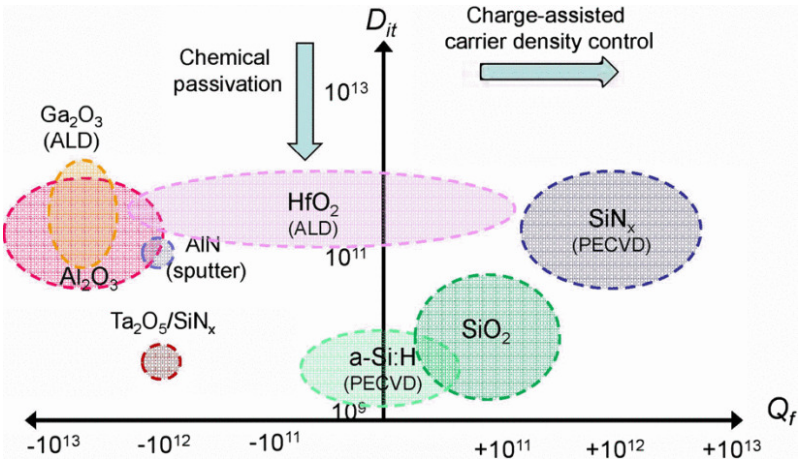

Figure 4.1. Summary of various passivation layers on Si in terms of D_{it} and Q_f [11].

The most successful dielectric material, which avoids mentioned issues, is aluminum oxide Al_2O_3. Al_2O_3 has a high negative charge density (Q_f) upon deposition on Si, provides an excellent passivation on p-type silicon surface [49]. The excellent passivation quality of the Al_2O_3 layer was attributed to a combination of negative charge density and low interface defect density, which stems from the usage of ALD [49].

Overall Al_2O_3 passivation of Si surface stems from a combination of both chemical and field-effect passivation [28]. Chemical passivation can be attributed due to a low interface defect (state) density D_{it} left after deposition [11]. Q_f and D_{it} of Al_2O_3 can be seen in mid left part of the graph depicted in Fig. 4.1.

At the same time, field-effect passivation can be attributed to the negative fixed charge density Q_f located within the c-Si/Al2O3 interface. The formation of fixed negative charge can be attributed to the thin interfacial layer of SiO_x that normally forms during the deposition between c-Si and Al2O3 [49]. This negative fixed charge density causes the desired imbalance in the carrier densities and the electrostatic potential within the region of Si towards the interface. The resulting depletion of electrons near the interface of c-Si/Al2O3 contributes to the excellent passivation quality of the Al_2O_3 [49]. Besides that, the previously mentioned ultrathin layer of SiO_x, generated by the oxidation step in the ALD and the residual hydrogen from the ALD process to achieve a low interface defect density of D_{it} of approx. 10^{11} cm^{-2} [7]. This SiO_x layer can be explicitly seen in Fig.4.2 done by tunneling electron microscope (TEM) [12].

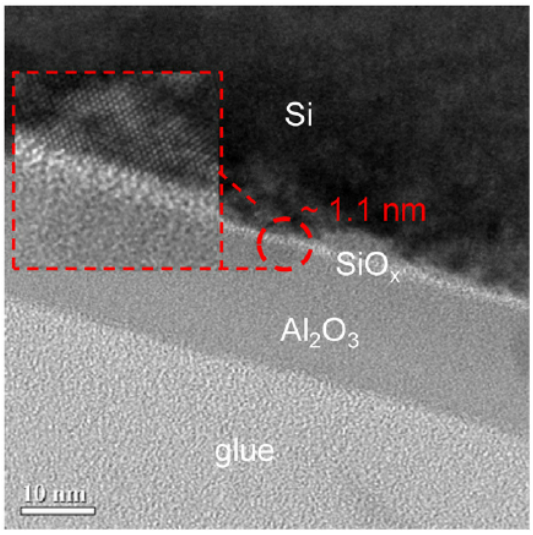

Figure 4.2. TEM image of a 15 nm Al_2O_3 film on c-Si after firing at peak temperature of 800°C [12].

Annealing is a rather important step that improves the passivation of Al_2O_3 film, both produced via thermal ALD and PEALD. For thermal ALD, annealing significantly improves the field-effect passivation while marginally improving the chemical passivation, whereas, for PEALD-produced films, annealing helps to increase the quality of chemical passivation [28]. It can be shown that post-deposition annealing can help to further reduce SRVs down to $2.4 cm.s^{-1}$ [50].

Overall low deposition temperatures of the ALD process are advantageous for the industrial fabrication of PV devices, which are, in general, are between 150°C and 250°C [28]. In general, both plasma-enhanced and thermal ALD led to surface recombination velocities below $10 cm.s^{-1}$ [49], however, an argument can be made that, even though higher throughput is achieved for PEALD, it is better to use thermal ALD

even at the loss of deposition rate and a slight increase of deposition temperature. C-Si/Al2O3 interface may be damaged during the PEALD process [49], thus reducing levels of the deposited film before the annealing process. Thermal ALD becomes a method of choice to deposit the passivation layer.

Best performing AlO_x passivation characteristics were demonstrated using PEALD, demonstrating S_{eff} as low as 0.26 and 0.95 cm.s^{-1} respectively for n- and p-type Si 1Ωcm [28]. This results are exceptional, however SRVs in the range of between 10cm.s^{-1} and 1cm.s^{-1} are regularly demonstrated for both thermal and PEALD [28, 49]. For example it was demonstrated that for p-type and lightly doped n-type Si wafers S_{eff} of 2cm.s^{-1} and 13cm.s^{-1} were achieved using PEALD with trimethylaluminum (TMA) and O_2 plasma as precursors [7]

Al_2O_3 ALD layer has been successfully used passivete B-doped (boron) emitters in n-type Si solar cells [51]. High power conversion rates of 23.2% have been achieved with this passivation layer. Another prominent application has been made in the industrial Passivated Emitter and Rear Cell (PERC) cell [52]. A combination of rear surface passivation via Al_2O_3 and a screen-printed aluminum local back surface field (BSF) have demonstrated a champion efficiency of 20.8% with further possible advancements up to 24%. ALD grown Al_2O_3 films have been successfully implemented in various commercial silicon solar cells.

Besides applications in silicon-based solar cells, the Al_2O_3 layer finds use in other applications, including other types of solar cells. Encapsulation and passivation of OPVs can be done by ALD Al_2O_3 layer. A conformal and uniform layer improves OPVs' stability and acts as a physical barrier protecting against atmospheric oxygen and water [7]. The stability of solar cells has improved significantly from 24h to 2000-7000h [7]. Low-temperature ALD process of Al2O3 can reduce the thermal impact on active organic layers, thus preventing efficiency losses when depositing as a separation layer between different stack layers Inspired by the application on c-Si solar cells, ALD Al_2O_3 has been successfully implemented in thin-film solar cells, such as CIGS and CZTS [7].

The aluminum oxide layer has been investigated as a promising high-k dielectric for the semiconductor industry [1]. Overall, the study of ALD Al_2O_3 growth is an excellent practice. Al_2O_3 is used in various applications for multiple types of solar cells and other dielectric-related applications in electronics.

Chapter 5
Growth and characterization

It is necessary to describe the equipment used in the deposition,pre-growth preparation, and growth procedure for the clearance and repeatability of the process. Characterization is then done to study conformality quality as well as effective lifetime τ_{eff} to assess passivation quality.

5.1 Overview of the equipment

Multiple complex apparatuses are involved in the deposition and characterization process of the metal oxide layer. Each of them requires a brief introduction and description.

5.1.1 Atomic layer deposition equipment

The ALD system installed in the Laboratory of Microelectronics of FEL, produced by SENTECH Instruments, is a SENTECH SI ALD system with Latch Lock (LL) and plasma source modification. This system is designed for small-scale production, which is ideal for research and development purposes in universities and other research facilities [53]. SI ALD system's key characteristics are reliability and the control software, and hardware flexibility, allowing for a wide range of deposition modes and processes. The SI ALD system allows for both thermal and plasma-enhanced deposition of metals, oxides, nitrides, and other chemical compounds.

The machine rack is the main component of the ALD system that contains the operational part of the system [54]. Machine rack of SI ALD system, installed in the laboratory comprises the reactor unit, the vacuum system, the gas and precursor cabinet (gas box), the control system, Load Lock with gate valve and load lock pump (LL), in-situ Real-Time Monitoring system (RTM) and true remote plasma source [53]. The reactor unit is equipped with a heating system that allows controlling the temperature of its walls.

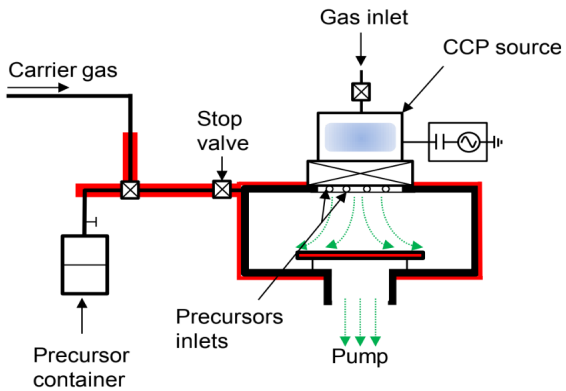

Figure 5.1. Princial scheme of the ALD [13]

Load Lock in the laboratory is expanded with the glove box compartment, MB200B produced by MBRAUN, which allows operating the wafer in a controlled, oxygen-free environment. A computer is required with the installed SENTECH software program and interface to operate the SI ALD system. Software is used to remotely control, using a pre-determined recipe, and monitor the whole deposition process, including loading of the substrate into the reactor unit. Various detectors are used to update the user with the current parameters of the deposition. The RF-powered plasma source is installed on top of the reactor unit. Under the reactor chamber, the vacuum system is located. It consists of a system of valves and a foreline pump. The whole system is responsible for creating and maintaining a vacuum at a particular pressure required for the deposition process. The process pressure is measured independent of process gas through an absolute pressure gauge (Baratron, MBA) [54].

In the SNECTECH SI ALD system process, gases and liquid precursors are supplied via a closed and exhausted gas and precursor cabinet, known as gas box [54]. Precursor dosing system components, including precursor lines and containers, are located in the lower part of the gas box. Usually, precursor dosing lines can be heated up to 200°C via heater jackets, and their temperature should be higher than the temperature of precursor containers. ALD system depending on the precursor properties, can utilize two different precursor dosing methods Direct Draw (DD) and Bubbling (B) [54]. As nitrogen may be used extensively for various purposes in the ALD system, a standard system has to be connected to a nitrogen supply. In the microelectronics, FEL, CTU nitrogen is guaranteed by the nitrogen generator Isocell PSA Nimos S2. The SENTECH SI ALD system is equipped with a CLEANSORB scrubber for the adsorption of waste gases made by CS Clean Solution. The figure 5.2 shows the complete system, with the glovebox installed in the laboratory.

Figure 5.2. SENTECH SI ALD system installed in the laboratory

ALD can be extended with RTM, an ellipsometer that can be used to in-situ monitor the growth of each layer, with a precision down to each step of a single cycle [13]. However, due to the shape of the wafer used in the deposition, RTM could not work correctly. Pyramidal-shaped surface prevented proper laser reflection and further analysis.

5.1.2 Atomic force microscope principles and equipment

An atomic force microscope (AFM) has been chosen to characterize the deposited Al_2O_3 layer in terms of uniformity and smoothness.

An atomic force microscope is one of the most prominent tools to study topography and various surface properties of materials with sub-nanometer precision. AFM belongs to a family of scanning probe microscope (SPM) [55] and can operate on a wide variety of conductive and non-conductive materials, including semiconductors, minerals, polymers, ceramics, composite glass, and biological materials [56]. AFM can also operate in various environments from ultrahigh vacuum to various fluids, thus making it a versatile tool used in science fields including solid-state physics, semiconductor studies, molecular biology, surface chemistry, etc [55].

Atomic force microscope works on principles of the surface and probe interactions that can be described based on continuum mechanics, the long-range van der Waals force, the capillary force, the short-range forces, the electrical double layer force in a liquid, and contamination effects [57]. Understanding principles behind tip-surface forces is substantial to achieving high-resolution scans. An AFM system generally consists of a probe, laser and position-sensitive photon-detector (PSPD), position controller, and a feedback system.

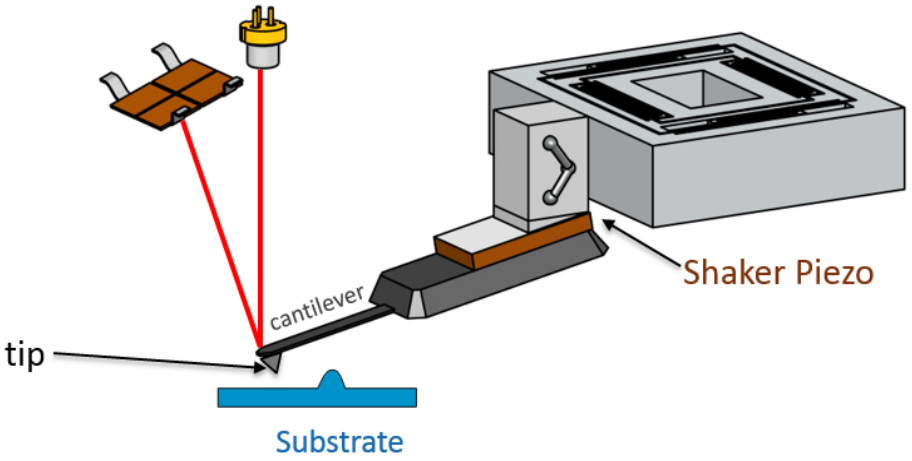

Figure 5.3. Princial scheme of the AFM [14]

The probe of AFM is an assembly of a highly sharp tip that is attached to the end of a narrow cantilever. A cantilever is generally made of silicon Si or silicon nitride Si_3N_4, making a softer cantilever with a lower spring constant [14]. The probe is usually moved using piezo elements or electrostatic micromanipulators that change its position in all three axes. As the probe scans across the investigated surface, its vertical and side-to-side motion is monitored by means of the laser beam reflected from the cantilever and the PSPD [14]. PSPD detects the motion and converts it to a signal that is then used in the feedback system and to analyze the studied material. Depending on the set parameter of the operational mode, the feedback system uses the signal from the PSPD and adjusts the probe's position via the vertical piezo element, so the set parameter is constant. Both the PSPD and the feedback system signals can be used to create a height profile and to analyze the studied qualities.

AFM can operate in a multitude of distinct modes with three main modes, depending on the type of the investigated material and desired parameters: contact mode, intermittent mode, and no-contact mode [57]. Contact mode is a relatively simple mode characterized by the probe being in contact with the surface during the scanning process. As set parameters, either height or interaction force can be chosen. Constant height mode uses laser reflection to plot the topography of the surface, while constant force mode uses a piezo element signal that adjusts the vertical position of the probe [57]. Intermittent (semi-contact) and no-contact modes are dynamic methods

that use a vibrating probe that is either amplitude or phase-modulated. Actuation of the cantilever is most commonly done by piezo-acoustic excitation or by photothermal excitation [14]. Amplitude modulated intermittent mode (AM-AFM) is a commonly used AFM imagining mode [58]. The cantilever is set to vibrate at the resonance frequency or near resonance frequency at a set amplitude, acting as a feedback parameter. As the tip comes closer to the surface, the oscillation amplitude is reduced due to tip-surface interaction forces. PSPD detects this reduction and sends a signal to the feedback system, adjusting the vertical probe position via piezo elements to return the amplitude to the set value. Signals sent by the feedback system can be used to create a 3D surface topology. Other dynamic modes may use phase or frequency as a set parameter. No-contact mode investigates the surface without touching it [57]. As the probe encounters the material, near-surface forces modify the oscillation, allowing the ability to investigate material properties and construct a surface profile. Dynamic modes provide additional benefits such as lessening the tip sharpness loss and decreasing potential surface damage [58]. Additional precision is added to the measurement in the intermittent mode since the usage of the oscillation amplitude as a set parameter allows to precisely tune probe-surface interactions.

Given a particular modification of a tip or of the interaction between the probe and a surface, AFM has a variety of methods to identify the compositional structure of the surface and to characterize mechanical (adhesion and stiffness), electrical (work function, capacitance), magnetic and optical properties of the materials [55]. Besides characterization, AFM can be used to manipulate, write or pull on substrates in lithography and molecular pulling experiments.

The atomic force microscope installed in the Laboratory of Microelectronics of FEL, produced by NT-MDT Spectrum Instruments, is NTEGRA ProbeNanoLaboratory (PNL). It is a versatile system that is able to perform contact AFM, semi-contact AFM, scanning tunneling microscopy (STM), and spectroscopy [59]. Both scannings by probe and scanning by the sample are available.

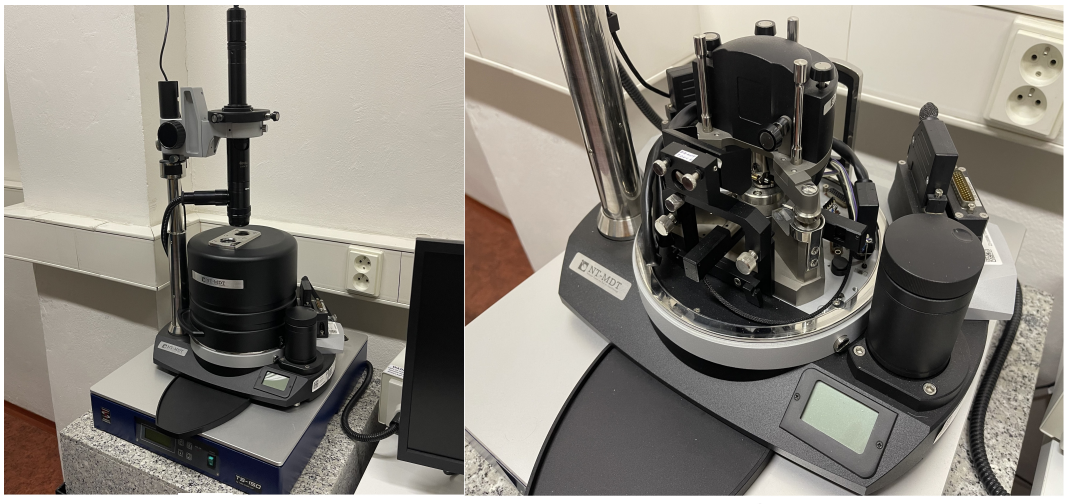

Figure 5.4. (a) NTEGRA AFM, (b) NT-MDT AFM base unit

It can be seen in Figure 5.4 (a) AFM is installed on the granite table and is covered with an insulation cap. This is done to phase out a noisy environment because AFM is extremely sensitive to vibration.

5.1.3 Effective lifetime measurements and equipment

Effective lifetime τ_{eff} is a practical parameter that can be used as a stand-alone characteristic of the PV device and also to calculate surface life time τ_s and subsequently S_{eff}. Effective lifetime is representative of the recombination rate of the solar cell. Measurements of this parameter can be done via a contactless and non-destructive method such as Photoconductance (PC) and Photoluminescence (PL) [60]. Equipment that has been used to conduct said measurements, produced by Sinton instruments, is Sinton WCT-120. The principal scheme can be observed in Fig. 5.5.

Derived from the continuity equation, effective lifetime, regardless of the illumination period can be calculated using general formula

$$\tau_{eff} = \Delta n_{avg}(t)/(G_{avg} - d\Delta n_{avg}(t)/dt),$$

where n_{avg} is the average excess carrier density and G_{avg} is the average generation rate [60]. Both parameters are can be determined on the laboratory equipment.

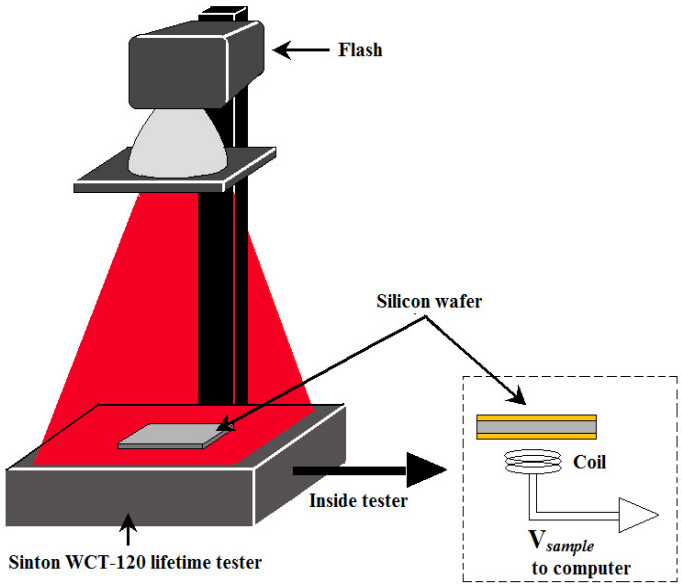

Figure 5.5. Principal scheme of Sinton WCT-120

Measurement is performed by illumination using a flash lamp onto the studied wafer, positioned over the conductive coil. Illumination stimulates photogeneration of charge carriers and, therefore, increases the wafer's conductance. The conductance change can be detected using a conductive coil and associated electronics [60]. Measured voltage levels associated with the conductance and the illumination parameters allow determining n_{avg} and G_{avg} that are then used to calculate τ_{eff}.

Lifetime measurement can be conducted in three distinct modes: quasi-steady-state (QSSPC), transient, and generalized lifetime analysis [60]. Transient PC mode uses short illumination period (in the range of microsecond) and it is assumed that the generation rate is zero. Effective lifetime is determined from the decay of signal using formula

$$\tau_{eff} = \Delta n_{avg}(t)/(-d\Delta n_{avg}(t)/dt)$$

On the other hand, QSSPC uses longer illumination periods so that the carrier density is constant $d\Delta n_{avg}(t)/dt = 0$ [60]. The formula transforms into

$$\tau_{eff} = \Delta n_{avg}(t)/(G_{avg}),$$

Generalized lifetime analysis uses a general formula to determine the needed parameter.

Sinton WCT-120 has a wide lifetime measurement range from 100ns to 10ms [61]. Sinton WCT-120 is a versatile tool, besides primary QSSPC and photo-conductance decay (PCD) measurements, it is available to conduct an examination of material quality and detection of heavy metals contamination during wafer processing evaluation of shunting, surface passivation, and substrate doping. Sinton WCT-120 system consists of a WCT-120 instrument, signal processing unit, and required Sinton software. A particular system, that was used in the experiment is shown in the Fig. 5.6.

Figure 5.6. Sinton WCT-120 in the laboratory with a Si wafer on it.

5.2 Deposition process

For the deposition process, Si n-type textured wafers were used, with a diameter of 50mm, a thickness of 140 μmeters, and base resistivity of more than 3 m$\Omega \cdot$ cm (measured resistivity was approximately 3.6 $\Omega \cdot$ cm depending on the wafer). Before deposition, wafers were subjected to a wet etching process to clean them and remove the intrinsic layer of SiO_2 formed on the surface. A chemical line for etching Si wafers, produced by STROZA, was used. The wet etching process consisted of sequential submersion of the wafers into the baths filled with NH_4OH+H_2O_2 mixture, HCl/H_2SO_4+H_2O_2 mixture and HF, divided by de-ionized (Di) water rinsing process. HF made Si surface hydrophobic.

To deposit Al_2O_3 on both sides of the wafer layer trimethylaluminium ($Al_2(CH_3)_6$) and water H_2O were used as precursors in the thermal ALD process with N_2 as the purge and carrier gas. Substrate heating was set to 200°C, whereas all the purge and precursor lines heating was set to 125°C. It was necessary to wait between depositions to stabilize wafer carrier temperature. The numbers of cycles, with respect to GPC of 0.08$\mathring{A}$, were 125 and 188, which lead to 10nm and 15 nm of thickness, respectively. Pressure in the chamber was set to be 9.7Pa, and as it can be seen in Fig. 5.7, the

set pressure varied between 9.5Pa and 12Pa, which was indicative of each step of each cycle.

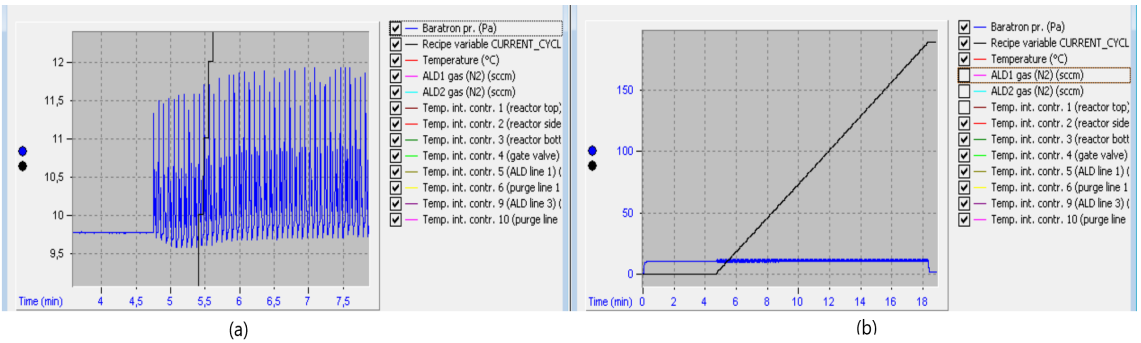

Figure 5.7. Graph of the reactor pressure and a number of cycles with relation to the time of the procedure; (a) enlarged part, (b) full graph.

Precursor exposure times were set to 120 ms, and the purge time period, with the 59 slm, was set to 2s. A summary of the main ALD deposition parameters is provided in a table 5.1 below. Fig. 5.8 shows Si wafer handling between deposition processes.

Parameters/Thickness	10nm	15nm
Temperature of the substrate	200°C	200°C
Temperature of purge and precursor lines	125°C	125°C
Number of ALD cycles	125	188
Chamber pressure	9.7Pa	9.7Pa
Precursor exposure period	120ms	120ms
Purge period	2s	2s

Table 5.1. Summary of ALD deposition

After the deposition samples were cooled and secured in the transportation box to be subjected for further studies.

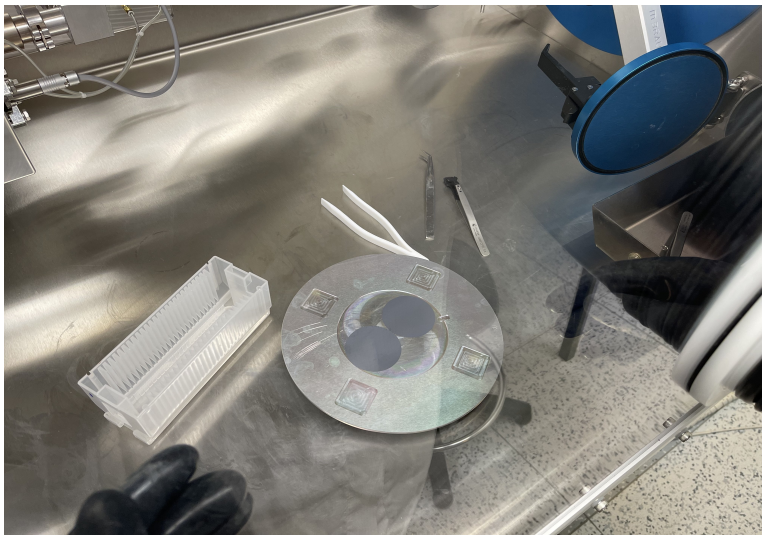

Figure 5.8. Si wafer with 15nm Al_2O_3 layer deposited on one side.

5.3 Characterization and results

5.3.1 Lifetime minority carrier measurements

Effective lifetime measurements were conducted on the Sinton WCT-120. τ_{eff} was measured on both wafers with 10nm and 15nm aluminum oxide layer approximately 10 minutes after the deposition and subsequently after more than 1 hour. For comparative purposes, effective lifetime was also measured on the Si wafer immediately after the wet etching process. Between measurements, wafers were kept in a deoxidized environment. Default Si wafer, according to technical documentation, has an effective lifetime of approximately 1μs. Application of 10nm and 15nm layers of Al_2O_3 have increased τ_{eff} up to 3.49μs and 1.95μs respectively, which indicates a slight improvement over default wafer lifetime. Table 5.2 shows that the effective lifetime of Al_2O_3 passivated wafers had further increased when they were later again tested, however, these results were still under the effective lifetime of Si wafer, which has undergone only wet etching process (6.01μs). Further study is required in order to propose an explanation of how storage in the deoxidized environment affects the effective lifetime of this particular combination of Al_2O_3 passivated Si wafers.

Wafer type/Time after deposition	approx. 10min.	approx. > 60min.
Si/Al_2O_3 layer of 10nm	3.49μs	4.02μs
Si/Al_2O_3 layer of 15nm	1.95μs	2.45μs
Default Si wafer	1μs	–
Si wafer after wet etching	6.01μs	–

Table 5.2. τ_{eff} effective lifetime measurements

These results could be seen as dim in comparison to results in other studies [12, 50], however, in those studies, different types of n-type Si wafers have been utilized. A further investigation is needed into the causes of the obtained τ_{eff} for this combination of the wafer and Al_2O_3 layer since many effects can change the surface recombination rate. In particular, in n-type Si, a negative charge of the passivation layer can create a near surface recombination channel that can, depending on the properties of the defects, reduce the effective lifetime at low injection levels [62]. τ_{eff} can also be dependent on the injection levels, and this dependence is affected by the size of the wafer [63]. The firing or annealing process could also be studied as it is suggested that these processes increase the effective carrier lifetime for a combination of Al_2O_3 and n-type Si wafers [49, 28, 12, 50].

Overall, passivation of textured n-type Si wafers with Al_2O_3 has increased effective carrier lifetime, but further studies are needed in order to understand how to improve obtained results for this wafer/layer case.

5.3.2 Atomic force microscopy measurements

AFM scans were conducted in semi-contact mode for both Si wafer and Si wafer passivated with Al_2O_3. A dense set of pyramid-shaped protuberances can be observed in AFM images from (b) Fig. 5.10 and Fig. 5.12. Fig. 5.9 (a) depicts a planar heatmap of a 700nm by 700nm area, whereas Fig. 5.9 (b) captures the slope of a particular pyramid in that area with a height of 0.45μm. The variability of heights and shapes of pyramid-like structures can be seen in images (b) and (c) of Fig. 5.10 and Fig. 5.12.

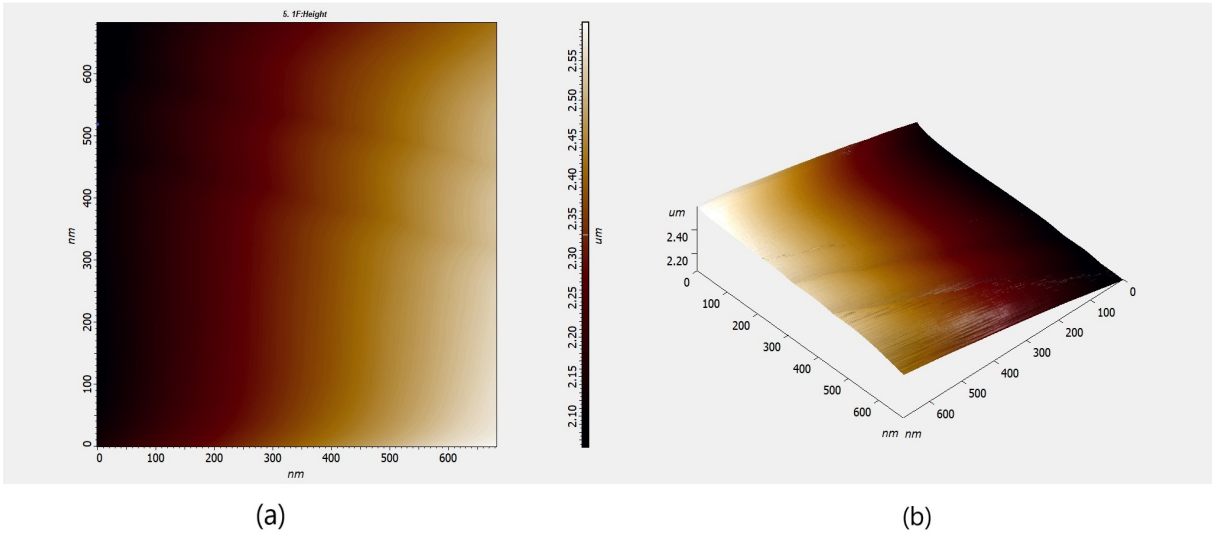

Figure 5.9. AFM scans of Si surface 0.7μm X 0.7μm, (a) planar surface heatmap, (b) 3D scan of the surface

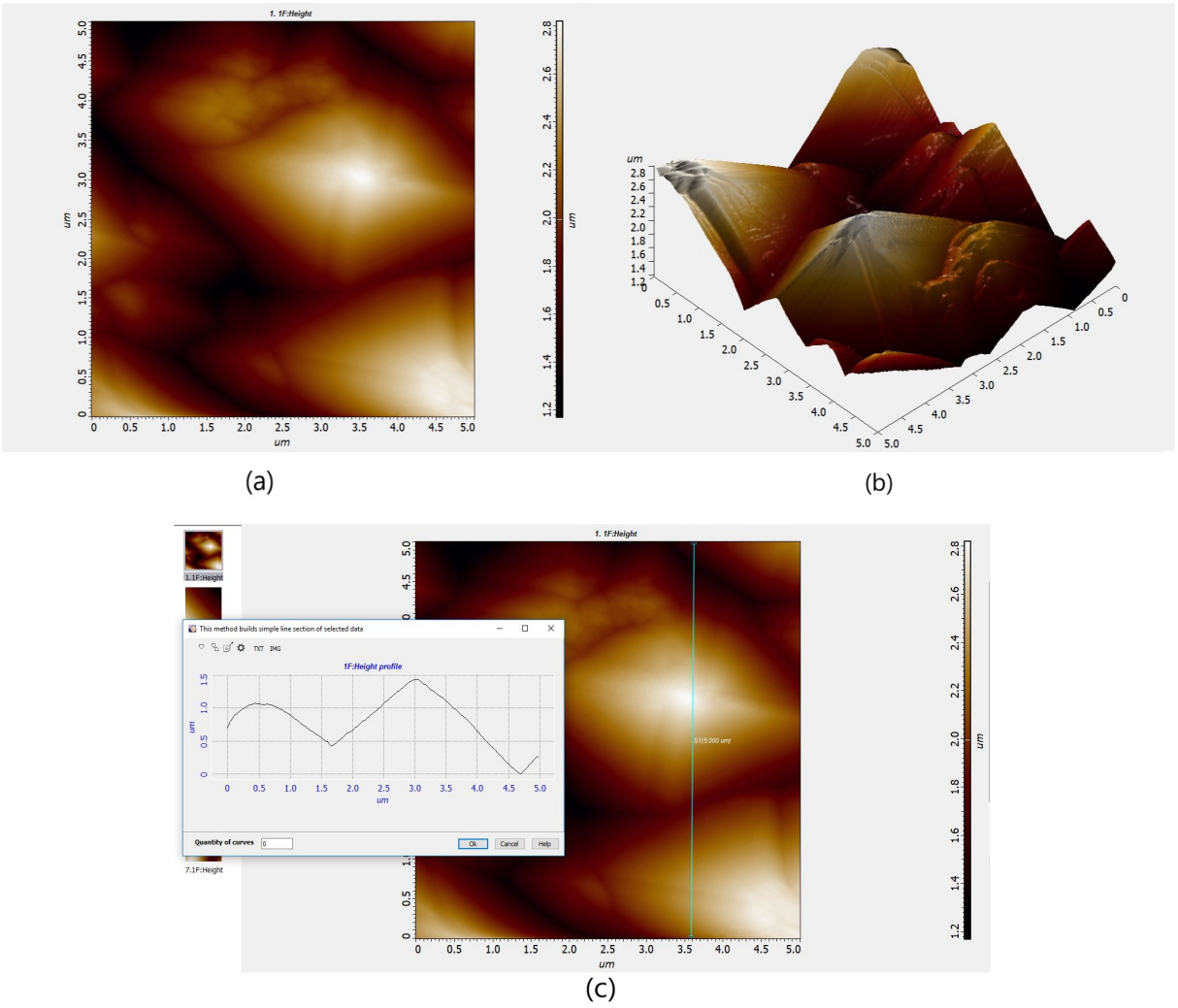

Figure 5.10. AFM scans of Al_2O_3 surface 5μm X 5μm, (a) planar surface heatmap, (b) 3D scan of the surface

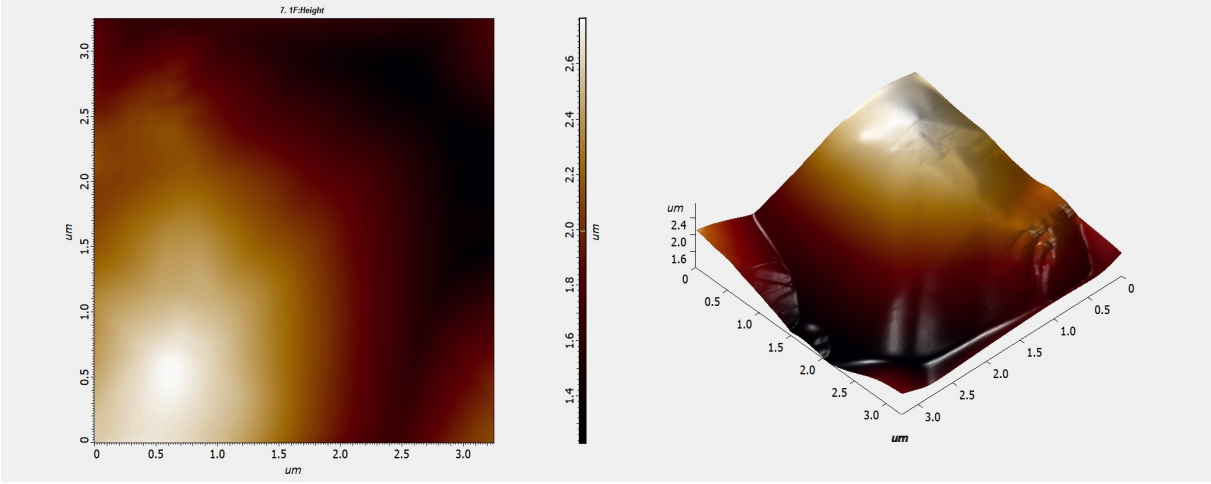

Figure 5.11. AFM scans of Al_2O_3 surface 3μm X 3μm, (a) planar surface heatmap, (b) 3D scan of the surface

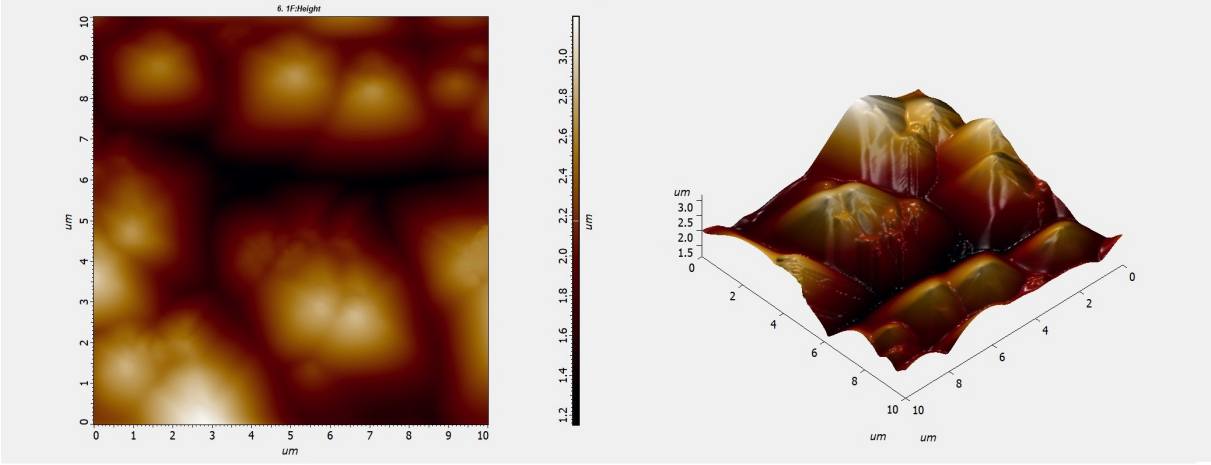

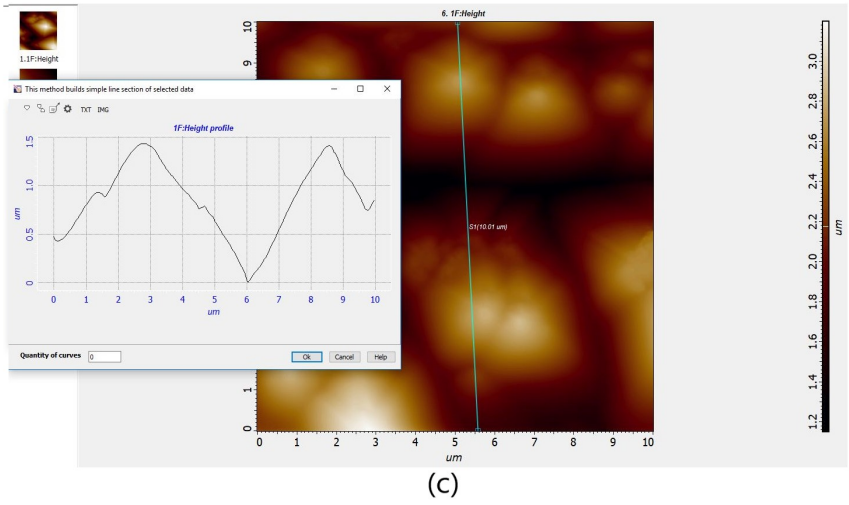

Figure 5.12. AFM scans of Al_2O_3 surface 10μm X 10μm, (a) planar surface heatmap, (b) 3D scan of the surface

The most prominent peak is approximately 2.85 μm . Planar images of Fig. 5.10 (a) and Fig. 5.12 (a) provide an excellent depiction of the surface and understanding of its topology. It can be seen in 3D scans of Fig. 5.9 (b) and Fig. 5.10 (b) that the surface of the Si exhibits a wavy roughness pattern. A conformal 10nm layer of Al_2O_3 smooths the surface by filling in the shallow troughs while maintaining the original surface texturing. Smoothing can be observed in Fig. 5.11 (b) and Fig. 5.12 (b). The same AFM images show how the ALD layer uniformly fills the areas between the pyramids and covers the surface, having the same color gradient across the slopes. In this case layer of Al_2O_3 provides chemical passivation covering the surface defects of the Si.

AFM images provide an excellent depiction of the wafer surface however it is difficult to indicate an increase of thickness of 10nm, because of the chosen scale of the scanning and of the fact that AFM scans have not been conducted in the same area of the wafer, which is technically problematic.

It is evident from the AFM pictures that the Al_2O_3 ALD layer has increased the uniformity of the surface, making it smoother, covering all the 3D topology elements. Textured surface is an example of relatively complex 3D topology and ALD, as expected, shows excellent conformality covering all surface trenches, slopes, and peaks.

Chapter 6
Conclusion

This thesis has introduced the Atomic Layer Deposition method, describing its characteristics, distinctive advantages, and specifications. A review of applications in photovoltaic device manufacturing was given, with applications spawning from relatively experimental ones that are studied by research groups around the world to already commercially established. Prior to the experimental part, a case was made for Al_2O_3 to be chosen to create a passivation layer for silicon-based solar cells, improving effective lifetime. In the experimental part of the thesis, deposition onto both sides of two Al_2O_3 layers of 10nm and 15 nm thickness onto silicon wafer was conducted. After characterization via AFM and effective lifetime measurements, it can be concluded that deposition was successful and that the passivation effect has been achieved, even considering the slight increase in the effective lifetime. Further studies are required to make the passivation effect better for the particular combination of wafer and passivation layer used in the experiment.

ALD is a precise and inherently self-limiting technique that produces highly conformal, reproducible pinhole-free thin films that can be uniformly deposited in complex 3D structures. ALD step-by-step procedure allows for precise thickness control and composition tunability. The utilization of ALD has further enabled miniaturization in electronics, including photovoltaic devices. ALD has helped to enable new solar cell architectures with thinner layers and more complex structures, thus allowing for the elimination of toxic and rare elements and increasing of power conversion. ALD is a vacuum process that can be integrated more easily into the standard manufacturing process, unlike CBD or wet etching. ALD provides better conformality, uniformity, and thickness control than other commonly used methods like CVD or PVD.

In order to progress further, ALD still needs to be improved. The older generation of chemistries struggle to provide a high quality of deposited films, lower temperatures, and good growth rates, or they hinder large-scale implementation, thus requiring the development of new generations of precursors made explicitly for the ALD process. As shown with photovoltaic devices, ALD has proven to be a successful technique in smaller-scale research tasks, but besides the commercially successful implementation of Al2O3 in the Si solar cell fabrication, ALD is still lacking in the commercial applications. The relatively slow deposition rate and cost-effectiveness should be addressed with new, higher-throughput ALD process modifications and improving already established modifications, such as spatial ALD that tries to solve the low deposition rate issue. Environmental sustainability should be in mind when developing new chemistries for ALD and modifying the process itself.

With all that said, ALD has a bright perspective ahead of it as a deposition technique since future technologies will capitalize on further miniaturization. With its myriad applications in numerous industries, ALD is on track to becoming a commonly implemented process in commercial production.

References

[1] Johnson, Richard W., Adam Hultqvist, and Stacey F. Bent. A brief review of atomic layer deposition: from fundamentals to applications. *Materials Today*. Elsevier BV, jun, 2014, Vol. 17, No. 5, pp. 236–246. Available from DOI 10.1016/j.mattod.2014.04.026. Available from https://doi.org/10.1016/j.mattod.2014.04.026.

[2] Knoops, H.C.M., S.E. Potts, A.A. Bol, and W.M.M. Kessels. *Atomic Layer Deposition*. Available from DOI 10.1016/b978-0-444-63304-0.00027-5. Available from https://doi.org/10.1016/b978-0-444-63304-0.00027-5.

[3] Arts, Karsten, Harvey Thepass, Marcel A. Verheijen, Riikka L. Puurunen, Wilhelmus M. M. Kessels, and Harm C. M. Knoops. Impact of Ions on Film Conformality and Crystallinity during Plasma-Assisted Atomic Layer Deposition of TiO_2. *Chemistry of Materials*. American Chemical Society (ACS), apr, 2021, Vol. 33, No. 13, pp. 5002–5009. Available from DOI 10.1021/acs.chemmater.1c00781. Available from https://doi.org/10.1021/acs.chemmater.1c00781.

[4] Kessels, W.M.M.. *Database of ALD processes*. Available from DOI 10.6100/ALD-DATABASE. Available from https://www.atomiclimits.com/alddatabase/.

[5] Kim, Hyungjun, Han-Bo-Ram Lee, and W.-J. Maeng. Applications of atomic layer deposition to nanofabrication and emerging nanodevices. *Thin Solid Films*. Elsevier BV, feb, 2009, Vol. 517, No. 8, pp. 2563–2580. Available from DOI 10.1016/j.tsf.2008.09.007. Available from https://doi.org/10.1016/j.tsf.2008.09.007.

[6] Yang, Xinbo, Peiting Zheng, Qunyu Bi, and Klaus Weber. Silicon heterojunction solar cells with electron selective TiO_x contact. *Solar Energy Materials and Solar Cells*. Elsevier BV, jun, 2016, Vol. 150, pp. 32–38. Available from DOI 10.1016/j.solmat.2016.01.020. Available from https://doi.org/10.1016/j.solmat.2016.01.020.

[7] Hossain, Md. Anower, Kean Thong Khoo, Xin Cui, Geedhika K Poduval, Tian Zhang, Xiang Li, Wei Min Li, and Bram Hoex. Atomic layer deposition enabling higher efficiency solar cells: A review. *Nano Materials Science*. Elsevier BV, sep, 2020, Vol. 2, No. 3, pp. 204–226. Available from DOI 10.1016/j.nanoms.2019.10.001. Available from https://doi.org/10.1016/j.nanoms.2019.10.001.

[8] Lindahl, J., J. T. Watjen, A. Hultqvist, T. Ericson, M. Edoff, and T. Torndahl. The effect of $Zn_{1-x}Sn_x)_y$ buffer layer thickness in 18.0% efficient Cd-free Cu(In, Ga)Se_2 solar cells. *Progress in Photovoltaics: Research and Applications*. Wiley, jul, 2012, Vol. 21, No. 8, pp. 1588–1597. Available from DOI 10.1002/pip.2239. Available from https://doi.org/10.1002/pip.2239.

[9] Kim. *Nanoscale*. The Royal Society of Chemistry, 2014, Vol. 6, pp. 14549-14554. Available from DOI 10.1039/C4NR04148H. Available from `http://dx.doi.org/10.1039/C4NR04148H`.

[10] Chang, Chih-Yu, Chun-Ting Chou, Yun-Jun Lee, Miin-Jang Chen, and Feng-Yu Tsai. Thin-film encapsulation of polymer-based bulk-heterojunction photovoltaic cells by atomic layer deposition. *Organic Electronics*. Elsevier BV, nov, 2009, Vol. 10, No. 7, pp. 1300–1306. Available from DOI 10.1016/j.orgel.2009.07.008. Available from `https://doi.org/10.1016/j.orgel.2009.07.008`.

[11] Cuevas, Andres, Thomas Allen, James Bullock, Yimao Wan, Di Yan, and Xinyu Zhang. Skin care for healthy silicon solar cells. In: *2015 IEEE 42nd Photovoltaic Specialist Conference (PVSC)*. 2015. pp. 1-6. Available from DOI 10.1109/PVSC.2015.7356379.

[12] Liao, Baochen, Rolf Stangl, Fa-Jun Ma, Thomas Mueller, Feifan Lin, Armin ABERLE, C Bhatia, and B. Hoex. Excellent c-Si surface passivation by thermal atomic layer deposited aluminum oxide after industrial firing activation. *Journal of Physics D: Applied Physics*. 09, 2013, Vol. 46, pp. 385102. Available from DOI 10.1088/0022-3727/46/38/385102.

[13] Gruska, B., H. Gargouri, and M. Arens. *Real Time True Surface Monitoring for ALD Processes*.

[14] AG, Nanosurf. *AFM operating principles*. Available from `https://www.nanosurf.com/en/support/afm-operating-principle`.

[15] Delft, J A van, D Garcia-Alonso, and W M M Kessels. Atomic layer deposition for photovoltaics: applications and prospects for solar cell manufacturing. *Semiconductor Science and Technology*. IOP Publishing, jun, 2012, Vol. 27, No. 7, pp. 074002. Available from DOI 10.1088/0268-1242/27/7/074002. Available from `https://doi.org/10.1088/0268-1242/27/7/074002`.

[16] Oviroh, Peter Ozaveshe, Rokhsareh Akbarzadeh, Dongqing Pan, Rigardt Alfred Maarten Coetzee, and Tien-Chien Jen. New development of atomic layer deposition: processes, methods and applications. *Science and Technology of Advanced Materials*. Informa UK Limited, may, 2019, Vol. 20, No. 1, pp. 465–496. Available from DOI 10.1080/14686996.2019.1599694. Available from `https://doi.org/10.1080/14686996.2019.1599694`.

[17] Puurunen, Riikka L.. A Short History of Atomic Layer Deposition: Tuomo Suntolas Atomic Layer Epitaxy. *Chemical Vapor Deposition*. Wiley, oct, 2014, Vol. 20, No. 10-11-12, pp. 332–344. Available from DOI 10.1002/cvde.201402012. Available from `https://doi.org/10.1002/cvde.201402012`.

[18] Ritala, Mikko, and Markku Leskela. Atomic Layer Deposition. In: H.S. NaZwa, ed. *Handbook of Thin Films Materials*. United Kingdom: Academic Press, 2002. pp. 103–159. ISBN 0-12-512909-2.

[19] Muneshwar, Triratna, Mengmeng Miao, Elham R. Borujeny, and Ken Cadien. *Atomic Layer Deposition*. Available from DOI 10.1016/b978-0-12-812311-9.00011-6. Available from `https://doi.org/10.1016/b978-0-12-812311-9.00011-6`.

[20] Johnson, Andrew L., and James D. Parish. *Recent developments in molecular precursors for atomic layer deposition*. Available from DOI 10.1039/9781788010672-00001. Available from `https://doi.org/10.1039/9781788010672-00001`.

[21] Miikkulainen, Ville, Markku Leskela, Mikko Ritala, and Riikka L. Puurunen. Crystallinity of inorganic films grown by atomic layer deposition: Overview and general trends. *Journal of Applied Physics*. AIP Publishing, jan, 2013, Vol. 113, No. 2, pp. 021301. Available from DOI 10.1063/1.4757907. Available from https://doi.org/10.1063/1.4757907.

[22] Muneshwar, Triratna, and Ken Cadien. Influence of atomic layer deposition valve temperature on ZrN plasma enhanced atomic layer deposition growth. *Journal of Vacuum Science & Technology A: Vacuum, Surfaces, and Films*. American Vacuum Society, nov, 2015, Vol. 33, No. 6, pp. 060603. Available from DOI 10.1116/1.4926382. Available from https://doi.org/10.1116/1.4926382.

[23] Leskela, Markku, and Mikko Ritala. Atomic Layer Deposition Chemistry: Recent Developments and Future Challenges. *Angewandte Chemie International Edition*. Wiley, nov, 2003, Vol. 42, No. 45, pp. 5548–5554. Available from DOI 10.1002/anie.200301652. Available from https://doi.org/10.1002/anie.200301652.

[24] Groner, M. D., F. H. Fabreguette, J. W. Elam, and S. M. George. Low-Temperature Al_2O_3 Atomic Layer Deposition. *Chemistry of Materials*. American Chemical Society (ACS), jan, 2004, Vol. 16, No. 4, pp. 639–645. Available from DOI 10.1021/cm0304546. Available from https://doi.org/10.1021/cm0304546.

[25] Guo, Zheng, Hao Li, Qiang Chen, Lijun Sang, Lizhen Yang, Zhongwei Liu, and Xinwei Wang. Low-Temperature Atomic Layer Deposition of High Purity, Smooth, Low Resistivity Copper Films by Using Amidinate Precursor and Hydrogen Plasma. *Chemistry of Materials*. American Chemical Society (ACS), aug, 2015, Vol. 27, No. 17, pp. 5988–5996. Available from DOI 10.1021/acs.chemmater.5b02137. Available from https://doi.org/10.1021/acs.chemmater.5b02137.

[26] Potts, S.E., and W.M.M. Kessels. Energy-enhanced atomic layer deposition for more process and precursor versatility. *Coordination Chemistry Reviews*. Elsevier BV, dec, 2013, Vol. 257, No. 23-24, pp. 3254–3270. Available from DOI 10.1016/j.ccr.2013.06.015. Available from https://doi.org/10.1016/j.ccr.2013.06.015.

[27] Böer. *Solar Cells*. Available from http://www.chemistryexplained.com/Ru-Sp/Solar-Cells.html.

[28] Bonilla, Ruy S., Bram Hoex, Phillip Hamer, and Peter R. Wilshaw. Dielectric surface passivation for silicon solar cells: A review. *physica status solidi (a)*. Wiley, jun, 2017, Vol. 214, No. 7, pp. 1700293. Available from DOI 10.1002/pssa.201700293. Available from https://doi.org/10.1002/pssa.201700293.

[29] Sreenivasan, Raghavasimhan, Paul C. McIntyre, Hyoungsub Kim, and Krishna C. Saraswat. Effect of impurities on the fixed charge of nanoscale HfO2 films grown by atomic layer deposition. *Applied Physics Letters*. AIP Publishing, sep, 2006, Vol. 89, No. 11, pp. 112903. Available from DOI 10.1063/1.2348735. Available from https://doi.org/10.1063/1.2348735.

[30] Palmstrom, Axel F., Pralay K. Santra, and Stacey F. Bent. Atomic layer deposition in nanostructured photovoltaics: tuning optical, electronic and surface properties. *Nanoscale*. Royal Society of Chemistry (RSC), 2015, Vol. 7, No. 29, pp. 12266–12283. Available from DOI 10.1039/c5nr02080h. Available from https://doi.org/10.1039/c5nr02080h.

[31] Pourret, Alexandre, Philippe Guyot-Sionnest, and Jeffrey W. Elam. Atomic Layer Deposition of ZnO in Quantum Dot Thin Films. *Advanced Materials*. Wiley, jan, 2009, Vol. 21, No. 2, pp. 232–235. Available from DOI 10.1002/adma.200801313. Available from https://doi.org/10.1002/adma.200801313.

[32] Oener, Sebastian Z., Alessandro Cavalli, Hongyu Sun, Jos E. M. Haverkort, Erik P. A. M. Bakkers, and Erik C. Garnett. Charge carrier-selective contacts for nanowire solar cells. *Nature Communications*. Springer Science and Business Media LLC, aug, 2018, Vol. 9, No. 1. Available from DOI 10.1038/s41467-018-05453-5. Available from https://doi.org/10.1038/s41467-018-05453-5.

[33] Zhang, Tian, Md. Anower Hossain, Chang-Yeh Lee, Yahya Zakaria, Amir A. Abdallah, and Bram Hoex. Atomic layer deposited $Zn_xNi_{1-x}O$: A thermally stable hole selective contact for silicon solar cells. *Applied Physics Letters*. AIP Publishing, dec, 2018, Vol. 113, No. 26, pp. 262102. Available from DOI 10.1063/1.5056223. Available from https://doi.org/10.1063/1.5056223.

[34] Scharber, M.C., and N.S. Sariciftci. Efficiency of bulk-heterojunction organic solar cells. *Progress in Polymer Science*. Elsevier BV, dec, 2013, Vol. 38, No. 12, pp. 1929–1940. Available from DOI 10.1016/j.progpolymsci.2013.05.001. Available from https://doi.org/10.1016/j.progpolymsci.2013.05.001.

[35] Hsu, Che-Chen, Heng-Wei Su, Cheng-Hung Hou, Jing-Jong Shyue, and Feng-Yu Tsai. Atomic layer deposition of NiO hole-transporting layers for polymer solar cells. *Nanotechnology*. IOP Publishing, aug, 2015, Vol. 26, No. 38, pp. 385201. Available from DOI 10.1088/0957-4484/26/38/385201. Available from https://doi.org/10.1088/0957-4484/26/38/385201.

[36] Roedern, Bolko von. How do Buffer Layers Affect Solar Cell Performance and Solar Cell Stability?. *MRS Proceedings*. Cambridge University Press, 2001, Vol. 668, pp. H6.9. Available from DOI 10.1557/PROC-668-H6.9.

[37] ILO, International Labour Organization. *International Chemical Safety Cards (ICSCs); Cadmium Sulfide*. Available from https://www.ilo.org/dyn/icsc/showcard.display?p_card_id=0404&p_version=1&p_lang=en##:~:text=Effects%20of%20long%2Dterm%20or,substance%20is%20carcinogenic%20to%20humans..

[38] Chaisitsak, Sutichai, Takeshi Sugiyama, Akira Yamada, and Makoto Konagai. $Cu(InGa)Se_2$ Thin-film Solar Cells with High Resistivity ZnO Buffer Layers Deposited by Atomic Layer Deposition. *Japanese Journal of Applied Physics*. IOP Publishing, sep, 1999, Vol. 38, No. Part 1, No. 9A, pp. 4989–4992. Available from DOI 10.1143/jjap.38.4989. Available from https://doi.org/10.1143/jjap.38.4989.

[39] Kato, Takuya. $Cu(In, Ga)(Se, S)_2$ solar cell research in Solar Frontier: Progress and current status. *Japanese Journal of Applied Physics*. IOP Publishing, feb, 2017, Vol. 56, No. 4S, pp. 04CA02. Available from DOI 10.7567/jjap.56.04ca02. Available from https://doi.org/10.7567/jjap.56.04ca02.

[40] Lockinger, Johannes, Shiro Nishiwaki, Christian Andres, Rolf Erni, Marta D. Rossell, Yaroslav E. Romanyuk, Stephan Buecheler, and Ayodhya N. Tiwari. ALD-Zn_xTi_yO as Window Layer in $Cu(In, Ga)Se_2$ Solar Cells. *ACS Applied Materials & Interfaces*. American Chemical Society (ACS), nov, 2018, Vol. 10, No. 50, pp. 43603–43609. Available from DOI 10.1021/acsami.8b14490. Available from https://doi.org/10.1021/acsami.8b14490.

[41] Nande, Amol, Swati Raut, and S.J. Dhoble. *Perovskite solar cells*. Available from DOI 10.1016/b978-0-12-823710-6.00002-9. Available from https://doi.org/10.1016/b978-0-12-823710-6.00002-9.

[42] Carcia, P.F., R.S. McLean, and Steven Hegedus. Encapsulation of Cu(InGa)Se_2 solar cell with Al_2O_3 thin-film moisture barrier grown by atomic layer deposition. *Solar Energy Materials and Solar Cells*. 2010, Vol. 94, No. 12, pp. 2375-2378. ISSN 0927-0248. Available from DOI https://doi.org/10.1016/j.solmat.2010.08.021. Available from https://www.sciencedirect.com/science/article/pii/S0927024810004782.

[43] Berger, Michael. *Two-dimensional (2D) materials*. Available from https://www.nanowerk.com/2D-materials.php.

[44] Antonova, I V. Chemical vapor deposition growth of graphene on copper substrates: current trends. *Physics-Uspekhi*. Uspekhi Fizicheskikh Nauk (UFN) Journal, oct, 2013, Vol. 56, No. 10, pp. 1013–1020. Available from DOI 10.3367/ufne.0183.201310i.1115. Available from https://doi.org/10.3367/ufne.0183.201310i.1115.

[45] Zhang, Yijun, Wei Ren, Zhuangde Jiang, Shuming Yang, Weixuan Jing, Peng Shi, Xiaoqing Wu, and Zuo-Guang Ye. Low-temperature remote plasma-enhanced atomic layer deposition of graphene and characterization of its atomic-level structure. *J. Mater. Chem. C*. The Royal Society of Chemistry, 2014, Vol. 2, pp. 7570-7574. Available from DOI 10.1039/C4TC00849A. Available from http://dx.doi.org/10.1039/C4TC00849A.

[46] Hao, W, C Marichy, and C Journet. Atomic layer deposition of stable 2D materials. *2D Materials*. IOP Publishing, oct, 2018, Vol. 6, No. 1, pp. 012001. Available from DOI 10.1088/2053-1583/aad94f. Available from https://doi.org/10.1088/2053-1583/aad94f.

[47] Kim, Hyun Gu, and Han-Bo-Ram Lee. Atomic Layer Deposition on 2D Materials. *Chemistry of Materials*. American Chemical Society (ACS), apr, 2017, Vol. 29, No. 9, pp. 3809–3826. Available from DOI 10.1021/acs.chemmater.6b05103. Available from https://doi.org/10.1021/acs.chemmater.6b05103.

[48] *About Nanotechnology*. Available from https://www.nano.gov/about-nanotechnology.

[49] Werner, Florian. *Atomic layer deposition of aluminum oxide on crystalline silicon: Fundamental interface properties and application to solar cells*. 2014. ISBN 978-3844030396.

[50] Barbos, Corina, Daniele Blanc-Pelissier, Alain Fave, Claude Botella, Philippe Regreny, Genevieve GRENET, Elisabeth Blanquet, Alexandre Crisci, and Mustapha Lemiti. Al2O3 thin films deposited by thermal atomic layer deposition: Characterization for photovoltaic applications. *Thin Solid Films*. Elsevier, 2016, Vol. 617, No. Part B, pp. 108-113. Available from DOI 10.1016/j.tsf.2016.02.049. Available from https://hal.archives-ouvertes.fr/hal-01712453.

[51] Benick, Jan, Bram Hoex, M. C. M. vande Sanden, W. M. M. Kessels, Oliver Schultz, and Stefan W. Glunz. High efficiency n-type Si solar cells on Al2O3-passivated boron emitters. *Applied Physics Letters*. AIP Publishing, jun, 2008, Vol. 92, No. 25, pp. 253504. Available from DOI 10.1063/1.2945287. Available from https://doi.org/10.1063/1.2945287.

[52] Huang, Haibing, Jun Lv, Yameng Bao, Rongwei Xuan, Shenghua Sun, Sami Sneck, Shuo Li, Chiara Modanese, Hele Savin, Aihua Wang, and Jianhua Zhao. Data of ALD Al2O3 rear surface passivation, Al2O3 PERC cell performance, and cell efficiency loss mechanisms of Al2O3 PERC cell. *Data in Brief*. 2017, Vol. 11, pp. 19-26. ISSN 2352-3409. Available from DOI https://doi.org/10.1016/j.dib.2016.12.030. Available from `https://www.sciencedirect.com/science/article/pii/S2352340916307910`.

[53] SENTECH, Instruments GMbH. *SI ALD LL, Atomic Layer Deposition with Load lock, Product description*.

[54] SENTECH, Instruments GMbH. *Atomic Layer Deposition System, SI ALD (LL), Operation Manual*.

[55] AG, Nanosurf. *History and Background of AFM*. Available from `https://www.nanosurf.com/en/support/history-and-background-of-afm`.

[56] Sinha Ray, Suprakas. *3 - Structure and Morphology Characterization Techniques*. Available from DOI https://doi.org/10.1016/B978-0-444-59437-2.00003-X. Available from `https://www.sciencedirect.com/science/article/pii/B9780444459437200003X`.

[57] Bellitto, Victor. *Atomic Force Microscopy*. Rijeka. Available from DOI 10.5772/2673. Available from `https://doi.org/10.5772/2673`.

[58] AG, Nanosurf. *AFM modes overview*. Available from `https://www.nanosurf.com/en/support/afm-modes-overview`.

[59] NT-MDT, Spectrum Instruments. *Instruction Manual for NTEGRA, Probe Nanolaboratory*.

[60] Grant, Nicholas. *Surface passivation and characterisation of crystalline silicon by wet chemical treatments*. 01, 2012. Ph.D. Thesis.

[61] Sinton, Instruments. *WCT-120 Offline Wafer Lifetime Measurement, Product Note*. Available from `https://www.sintoninstruments.com/wp-content/uploads/Sinton-WCT-120-product-note.pdf`.

[62] Dirnstorfer, Ingo, Daniel K Simon, Paul M Jordan, and Thomas Mikolajick. Near surface inversion layer recombination in Al_2O_3 passivated n-type silicon. *J. Appl. Phys.* AIP Publishing, jul, 2014 , Vol. 116, No. 4, pp. 044112.

[63] Veith, Boris, Tobias Ohrdes, Florian Werner, Rolf Brendel, Pietro P. Altermatt, Nils-Peter Harder, and Jan Schmidt. Injection dependence of the effective lifetime of n-type Si passivated by Al2O3: An edge effect?. *Solar Energy Materials and Solar Cells*. 2014, Vol. 120, pp. 436-440. ISSN 0927-0248. Available from DOI https://doi.org/10.1016/j.solmat.2013.06.049. Available from `https://www.sciencedirect.com/science/article/pii/S0927024813003449`.